

1 **Inputs and processes affecting the distribution of**
2 **particulate iron in the North Atlantic along the GEOVIDE**
3 **(GEOTRACES GA01) section**

4
5
6 Arthur Gourain^{1,2}, Hélène Planquette¹, Marie Cheize^{1,3}, Nolwenn Lemaitre^{1,4}, Jan-Lukas
7 Menzel Barraqueta⁵, Rachel Shelley^{1,6}, Pascale Lherminier⁷ and Géraldine Sarthou¹

8
9 1-UMR 6539/LEMAR/IUEM, Technopôle Brest Iroise, Place Nicolas Copernic, 29280 Plouzané, France

10 2- now at Ocean Sciences Department, School of Environmental Sciences, University of Liverpool, Liverpool,
11 L69 3GP, United Kingdom

12 3- now at Ifremer, Centre de Brest, Géosciences Marines, Laboratoire des Cycles Géochimiques (LCG), 29280
13 Plouzané, France

14 4- now at Department of Earth Sciences, Institute of Geochemistry and Petrology, ETH-Zürich, Zürich,
15 Switzerland

16 5- GEOMAR, Helmholtz Centre for Ocean Research Kiel, Wischhofstraße 1-3, 24148 Kiel, Germany

17 6- now at Earth, Ocean and Atmospheric Science, Florida State University, Tallahassee, Florida, 32310, USA

18 7- Ifremer, LPO, UMR 6523 CNRS/Ifremer/IRD/UBO, Ifremer Centre de Brest, CS 10070, Plouzané, France

19
20 *Correspondence to: helene.planquette@univ-brest.fr*

21
22 **Abstract**

23 The GEOVIDE cruise (May-June 2014, R/V Pourquoi Pas?) aimed to provide a better understanding on trace
24 metal biogeochemical cycles in the North Atlantic. As particles play a key role in the global biogeochemical
25 cycle of trace elements in the ocean, we discuss the distribution of particulate iron (PFe), in light of particulate
26 aluminium (PAI), manganese (PMn) and phosphorus (PP) distributions. Overall, 32 full vertical profiles were
27 collected for trace metal analyses, representing more than 500 samples. This resolution provides a solid basis for
28 assessing concentration distributions, elemental ratios, size-fractionation, or adsorptive scavenging processes in
29 key areas of the thermohaline circulation. Total particulate iron (PFe) concentrations ranged from as low as 9
30 pmol L⁻¹ in surface Labrador Sea waters to 304 nmol L⁻¹ near the Iberian margin, while median PFe
31 concentrations of 1.15 nmol L⁻¹ were measured over the sub-euphotic ocean interior.

32 Within the Iberian Abyssal Plain, ratio of PFe over particulate aluminium (PAI) is identical to the continental
33 crust ratio (0.21), indicating the important influence of crustal particles in the water column.~~At most stations~~
34 ~~over the Western, the relative concentrations of total PFe and aluminium (PAI) showed the near ubiquitous~~
35 ~~influence of crustal particles in the water column.~~ Overall, the lithogenic component explained more than 87%
36 of PFe variance along the section. Within the Irminger and Labrador basins, the formation of biogenic particles
37 led to an increase of the PFe/PAI ratio (up to 0.7 mol mol⁻¹) compared to the continental crust ratio (0.21 mol

38 mol⁻¹), Margins provide important quantities of particulate trace elements (up to 10 nmol L⁻¹ of PFe) to the open
39 ocean, and in the case of the Iberian margin, advection of PFe was visible more than 250km away from the
40 margin. Additionally, several benthic nepheloid layers spreading over 200m above the seafloor were
41 encountered along the transect, especially in the Icelandic, Irminger and Labrador basins, delivering particles
42 with high PFe content, up to 89 nmol L⁻¹ of PFe. Finally, remineralisation processes are also discussed, and
43 showed different patterns among basins and elements.

44

45 **1. Introduction**

46 Particles play a key role in the ocean where they drive the residence time of most elements (Jeandel et al., 2015),
47 and strongly influence the global biogeochemistry of macro and micro-nutrients including iron (Milne et al.,
48 2017). In the surface ocean, biological activity produces biogenic suspended matter through planktonic
49 organisms, while atmospheric deposition (Baker et al., 2013; Jickells et al., 2005), riverine discharge (Aguilar-
50 Islas et al., 2013; Berger et al., 2008; Ussher et al., 2004) or ice-melting (Hawkings et al., 2014; Lannuzel et al.,
51 2011, 2014) bring mostly lithogenic derived particles to surface waters. These particulate inputs highly vary,
52 both spatially and seasonally, around the world's oceans. At depth, benthic and shelf sediment resuspension
53 (e.g. Aguilar-Islas et al., 2013; Cullen et al., 2009; Elrod et al., 2004; Fitzwater et al., 2000; Hwang et al., 2010;
54 Lam et al., 2015; Lam and Bishop, 2008; McCave and Hall, 2002), and hydrothermal activity (Elderfield and
55 Schultz, 1996; Lam et al., 2012; Tagliabue et al., 2010, 2017; Trefry et al., 1985), provides important amounts
56 of particles to the water column. Moreover, authigenic particles can be produced *in-situ* by aggregation of
57 colloids (Bergquist et al., 2007) or oxidation processes (Bishop and Fleisher, 1987; Collier and Edmond, 1984).
58 Thus, oceanic particles result from a complex combination of these different sources and processes (Lam et al.,
59 2015).

60 Particles represent the main part of the total iron pool in the upper water column (Radic et al., 2011), and
61 strongly interact with the dissolved pool (e.g. Ellwood et al., 2014). Indeed, dissolved iron can be scavenged
62 onto particles (Gerringa et al., 2015; Rijkenberg et al., 2014), incorporated into biogenic particles (Berger et al.,
63 2008) or ~~produced by remineralisation of particles~~ (Dehairs et al., 2008; Sarthou et al., 2008). Interestingly,
64 the concept of “reversible scavenging” (i.e. release at depth of dissolved iron previously scavenged onto
65 particles) has been advocated recently (Dutay et al., 2015; Jeandel and Oelkers, 2015; Labatut et al., 2014),
66 while other studies reveal distinct dissolution processes (e.g. Oelkers et al., 2012; Cheize et al., submitted to
67 Chemical Geology). Slow dissolution of particulate iron at margins has also been evoked as a continuous
68 fertilizer of primary production and should be considered as a source of dissolved iron (e.g. Jeandel et al., 2011;
69 Jeandel and Oelkers, 2015; Lam and Bishop, 2008). Within or below the mixed layer, the rates of regeneration
70 processes can also impact the bioavailable pool of iron, among other trace metals (e.g. Ellwood et al., 2014;
71 Nuester et al., 2014). However, the rates of these processes are not yet fully constrained. The study of particulate
72 iron is thus essential to better constrain the global biogeochemical cycle of iron in the ocean. This subject
73 received a growing interest over the last 10 years in particular (e.g. Bishop and Biscaye, 1982; Collier and
74 Edmond, 1984; Frew et al., 2006; Lam et al., 2012; Milne et al., 2017; Planquette et al., 2011, 2013; Sherrell et
75 al., 1998) and, to our knowledge, only two have been performed at an ocean-wide scale and published so far: the
76 GA03 GEOTRACES North Atlantic Zonal Transect (Lam et al., 2015; Ohnemus and Lam, 2015) and the GP16
77 GEOTRACES Pacific Transect (Lam et al., 2017; Lee et al., 2017).

78 In this context, this paper presents the particulate iron distribution in the North Atlantic Ocean, along the
79 GEOTRACES GA01 section (GEOVIDE), and discusses the various sources and processes affecting its
80 distribution, using ~~the distribution of other trace elements, more particularly~~ particulate aluminium, phosphorus
81 or manganese, ~~to further our understanding of this important pool of iron.~~
82

83 2. Methods

84 2.1. Study area

85 Particulate samples were collected at 32 stations during the GEOVIDE (GEOTRACES GA01 section) campaign
86 between May and June 2014 aboard the R/V *Pourquoi Pas?* in the North Atlantic. The sampling spanned
87 several biogeochemical provinces (Figure 1): ~~that first comprised~~ the Iberian margin (IM, Stations 2, 1 and 4),
88 the Iberian Abyssal Plain (IAP, Stations 11 to 17), the Western European Basin (WEB, Station 19 to Station 29)
89 ~~and;~~ the Icelandic Basin (IcB, Stations 32 to 36). ~~Then, samples were collected;~~ above the Reykjanes Ridge (RR,
90 Station 38), ~~in~~ the Irminger Basin (IrB, Stations 40 to 60), ~~close to~~ the Greenland shelf (GS, Stations 53 and 61),
91 the Labrador Basin (LB, Stations 63 to 77) and finally ~~close~~ the Newfoundland shelf (NS, Station 78) (Figure
92 1).

93 The North Atlantic is characterized by a complex circulation (briefly described in section 2.1 and in detail by
94 Zunino et al. (2017) and García-Ibáñez et al. (2015) and is one of the most productive regions of the global
95 ocean (Martin et al., 1993; Sanders et al., 2014), with a complex phytoplankton community structure composed
96 of diverse taxa (Tonnard et al., in prep.).
97

98 2.2. Sampling

99
100 Samples were collected using the French GEOTRACES clean rosette, equipped with twenty-two 12L GO-FLO
101 bottles (two bottles were leaking and were never deployed during the cruise). GO-FLO bottles (~~General~~
102 ~~Oceanics~~) were initially cleaned in the home laboratory (LEMAR) following the GEOTRACES procedures
103 (Cutter and Bruland, 2012). The rosette was deployed on a ~~146~~mm Kevlar cable with a dedicated, custom-
104 designed clean winch. Immediately after recovery, the GO-FLO bottles were individually covered at each end
105 with plastic bags to minimize contamination. They were then transferred into a clean container (class-100) for
106 sampling, and the filters processed under a laminar flow unit. On each cast, nutrient and/or salinity samples
107 were taken to check potential leakage of the GO-FLO bottles.

108 ~~Prior to filtration, Filters were cleaned following the GEOTRACES protocols~~
109 ~~(<http://www.geotraces.org/images/Cookbook.pdf>) and kept in acid-cleaned 1 L LDPE bottles (Nalgene) filled~~
110 ~~with ultrapure water (Milli-Q, resistivity of 18.2 MΩ cm) until use. All filters were 25 mm diameter in order to~~
111 ~~optimize signal over the filter blank except at the surface depth where 47 mm diameter filters mounted on acid-~~
112 ~~cleaned polysulfone filter holders (Nalgene™) were used. Prior to filtration, the GO-FLO bottles were shaken~~
113 three times, as recommended in the GEOTRACES cookbook to avoid settling of particles in the lower part of
114 the bottle. GO-FLO bottles were pressurized to <8 psi with 0.2 μm filtered dinitrogen (N₂, Air Liquide).
115 Seawater was then filtered directly through paired filters (Pall Gelman Supor™ 0.45 μm polyetersulfone, and
116 Millipore mixed ester cellulose MF 5 μm) mounted in Swinnex polypropylene filter holders (Millipore),

117 following Planquette and Sherrell (2012) inside the clean container. Filtration was operated until the bottle was
118 empty or until the filter clogged; volume filtered ranged from 2 liters for surface samples to 11L within the
119 water column. ~~Filters were cleaned following the protocol described in Planquette and Sherrell (2012) and kept
120 in acid-cleaned 1 L LDPE bottles (Nalgene) filled with ultrapure water (Milli-Q, resistivity of 18.2 M Ω cm⁻³)
121 until use. All filters were 25 mm diameter in order to optimize signal over the filter blank except at the surface
122 depth where 47 mm diameter filters mounted on acid-cleaned polysulfone filter holders (Nalgene™) were used.~~
123 After filtration, filter holders were disconnected from the GO-FLO bottles and a gentle vacuum was applied
124 using a syringe in order to remove any residual water under a laminar flow hood. Filters were then removed
125 from the filter holders with plastic tweezers that were rinsed with Milli-Q between samples. Most of the
126 remaining seawater was ‘sipped’ by capillary action, when placing the non-sampled side of the filter onto a
127 clean 47 mm supor filter. Then, each filter pair was placed in an acid-cleaned polystyrene Petri~~Slides~~-slide
128 (Millipore), double bagged, and finally stored at -20°C until analysis at LEMAR. Between casts, filter holders
129 were thoroughly rinsed with Milli-Q, placed in an acid bath (5% HCl) for 24 hours, then rinsed with Milli-Q.
130 At each station, process blanks were collected as follows: 2L of a deep (1000 m) and a shallow (40 m) seawater
131 samples were first filtered through a 0.2 μ m pore size capsule filter (Pall Gelman Acropak 200) mounted on the
132 outlet of the GO-FLO bottle before to pass through the particle sampling filter, which was attached directly to
133 the swinnex filter holder.

134

135 *2.3. Analytical methods*

136 Back in the home laboratory, sample handling was performed inside a clean room (Class 100). All solutions
137 were prepared using ultrapure water (Milli-Q) and all plasticware had been acid-cleaned before use. Frozen
138 filters, collected within the mixed layer depth or within nepheloid layers, were first cut in half using a ceramic
139 blade: one filter half was dedicated to total digestion (see below), while the other half was archived at -20°C for
140 SEM analyses or acid leaching of “labile” metals (Berger et al., 2008; to be published separately).

141 Filters were digested following the method described in Planquette and Sherrell (2012). Filter were placed on
142 the inner wall of acid-clean 15mL PFA vials (Savillex™), and 2 mL of a solution containing 2.9 mol L⁻¹
143 hydrofluoric acid (HF, suprapur grade, Merck) and 8 mol L⁻¹ nitric acid (HNO₃, Ultrapur grade, Merck) was
144 added to each vial. Vials were then closed and refluxed at 130°C on a hot plate for 4 hours. After cooling, the
145 digest solution was evaporated at 110°C until near dryness. Then, 400 μ L of concentrated HNO₃ (Ultrapur
146 grade, Merck) was added, and the solution was re-evaporated at 110°C. Finally, the obtained residue was
147 dissolved with 3mL of a 0.8 mol L⁻¹ HNO₃ (Ultrapure grade, Merck). This archive solution was transferred to an
148 acid cleaned 15 mL polypropylene centrifuge tube (Corning®) and stored at 4°C until analyses.

149 All analyses were performed on a sector field inductively coupled plasma mass spectrometer (SF-ICP-MS
150 Element2, Thermo-Fisher Scientific). Samples were diluted by a factor of 7 on the day of analysis in acid-
151 washed 13 mm (outer diameter) rounded bottom, polypropylene centrifuge tubes (VWR) with 0.8 mol L⁻¹ HNO₃
152 (Ultrapur grade, Merck) spiked with 1 μ g L⁻¹ of Indium (¹¹⁵In) solution in order to monitor the instrument drift.
153 Samples were introduced with a PFA-ST nebulizer connected to a quartz cyclonic spray chamber (Elemental
154 Scientific Incorporated, Omaha, NE) via a modified SC-Fast introduction system consisting of an SC-2
155 autosampler, a six-port valve and a vacuum-rinsing pump. The autosampler was contained under a HEPA
156 filtered unit (Elemental Scientific). Two 6-points, matrix-matched multi-element standard curves with

157 concentrations bracketing the range of the samples were run at the beginning, the middle and the end of each
158 analytical run. Analytical replicates were made every 10 samples, while accuracy was determined by performing
159 digestions of the certified reference material BCR-414 (plankton, Community Bureau of Reference,
160 Commission of the European Communities), PACS-3 and MESS-4 (marine sediments, National Research
161 Council Canada), following the same protocol as for samples. Recoveries were typically within 10% of the
162 certified values (and within the error of the data, taken from replicate measurements, Table 1). Once all data
163 were normalized to an ^{115}In internal standard and quantified using an external standard curve, the dilution factor
164 of the total digestion was accounted for. Obtained element concentrations per filter (pmol/filter) were then
165 corrected by the process blanks described above. Finally, pmol/filter values were divided by the volume of
166 water filtered through stacked filters.

167 Total concentrations (sum of small size fraction (0.45-5 μm) and large (>5 μm) size fraction) of particulate trace
168 elements are reported in Table S1 (supplementary data).

169

170

171

2.4. Ancillary data:

172 ~~Particulate barium (Ba) concentrations were determined in samples collected using a standard CTD rosette~~
173 ~~equipped with 12 L Niskin bottles. Typically, 18 samples were collected at each station within the first 1000 m.~~
174 ~~Details on analytical procedures are given in Lemaitre et al. (in press, 2018a). Briefly, particulate biogenic~~
175 ~~Barium, or excess Barium (Ba_{ex}), were calculated by subtracting the particulate lithogenic barium (PBa-litho)~~
176 ~~from the total particulate barium (PBa). The PBa-litho was determined by multiplying the particulate aluminium~~
177 ~~(PAI) concentration by the upper continental crust (UCC) Ba: Al molar ratio (0.00135 mol mol $^{-1}$; Taylor and~~
178 ~~McLennan, 1985). Potential temperature (θ), salinity (S), and transmissometry data were retrieved from the CTD~~
179 ~~sensors (CTD SBE911 equipped with a SBE43).~~

180

181

2.5. Positive matrix factorisation

182 Positive Matrix Factorisation (PMF) was run to characterise the main factors influencing the particulate trace
183 elements variances along the GEOVIDE section. In addition to PFe, PAI, PMn, and PP, nine additionnal
184 elements were included in the PMF: Y, Ba, Pb, Th, Ti, V, Co, Cu and Zn. The analysis has been conducted on
185 samples where all the 13 elements previously cited were above the detection limits; after selection, 445 of the
186 549 existing data points were used. Analyses were performed using the PMF software, EPA PMF 5.0,
187 developed by the USA Environmental Protection Agency (EPA). Models have been tested with several factors
188 number (from 3 to 6), after full error estimation of each model, we decide to use the configuration providing the
189 lowest errors estimations and in consequence the most reliable.
190 In consequence, models were set up with four factors and were run 100 times to observe the stability of the
191 obtained results. After displacement, error estimations and bootstraps error estimations, the model was
192 recognised as stable.

193

194

3. Results

195

3.1. Hydrography and biological setting

196 Here, we briefly describe the hydrography encountered during the GEOVIDE section (Figure 2), as a thorough
197 description is available in García-Ibáñez et al. (2015). The warm and salty Mediterranean Water (MW, $S=36.50$,
198 $\theta=11.7^{\circ}\text{C}$) was sampled between 600 and 1700 m in the Iberian Abyssal Plain (IAP). MW resulted from the
199 mixing between the Mediterranean Overflow Water plume coming from the Mediterranean Sea and local
200 waters. Surface water above the Iberian Shelf was characterised by low salinity ($S=34.95$) at station 2 and 4
201 compared to surrounding water masses. Close to the floor of the Iberian Abyssal Basin, the North East Atlantic
202 Deep Water (NEADW, $S=34.89$, $\theta=2.0^{\circ}\text{C}$) spread southward. The ~~East~~–North Atlantic Central Water
203 (~~EN~~ACW, $S>35.60$, $\theta>12.3^{\circ}\text{C}$) was the warmest water mass of the transect and was observed in the subsurface
204 layer of the Western European Basin and Iberian Abyssal Plain. An old Labrador Sea Water (LSW, $S=34.87$,
205 $\theta=3.0^{\circ}\text{C}$) flowed inside the Western European and Icelandic Basins, between 1000 and 2500m depth. In the
206 Icelandic Basin, below the old LSW, the Iceland-Scotland Overflow Water (ISOW, $S=34.98$, $\theta=2.6^{\circ}\text{C}$) spread
207 along the Reykjanes Ridge slope. This cold water, originating from the Arctic, led to the formation of NEADW
208 after mixing with surrounding waters. North Atlantic hydrography was impacted by the northward flowing of
209 the North Atlantic Current (NAC), which carried up warm and salty waters from the subtropical area. When
210 NAC crossed the Mid-Atlantic ridge through the Charlie-Gibbs Fracture Zone (CGFZ), it created the Subpolar
211 Mode Water (SPMW). The recirculation of SPMW inside the Icelandic and Irminger Basins led to the formation
212 of regional modal waters: the Iceland Subpolar Mode Water (IcSPMW, $S=35.2$, $\theta=8.0^{\circ}\text{C}$) and the Irminger
213 Subpolar Mode Water (IrSPMW, $S=35.01$, $\theta=5.0^{\circ}\text{C}$) respectively. IcSPMW was a relatively warm water mass
214 with potential temperature up to 7°C (García-Ibáñez et al., 2015). Another branch of the NAC mixed with
215 Labrador Current waters to form the relatively fresh SubArctic Intermediate Water (SAIW, $S<34.8$,
216 $4.5^{\circ}\text{C}<\theta<6^{\circ}\text{C}$). The Irminger Basin is a ~~really~~-complex area with a multitude of water masses. In the middle of
217 the basin, an old LSW, formed one year before (Straneo et al., 2003), spread between 500 and 1200 m depth.
218 Close to the bottom, the Denmark Strait Overflow Water (DSOW, $S=34.91$) flowed across the basin. Greenland
219 coastal waters were characterised by low salinity values, down to $S=33$. The strong East Greenland Current
220 (EGC) flowed southward along the Greenland shelf in the Irminger Basin. When reaching the southern tip of
221 Greenland, this current entered the Labrador Basin along the west coast of Greenland and followed the outskirts
222 of the basin until the Newfoundland shelf. In the Labrador Basin, the deep convection of SPMW at 2000 m was
223 involved in the formation of the LSW ($S=34.9$, $\theta=3.0^{\circ}\text{C}$) (García-Ibáñez et al., 2015; Yashayaev and Loder,
224 2009). Above the Newfoundland Shelf, surface waters were affected by discharge from rivers and ice-melting
225 and characterised by extreme low salinity for open ocean waters, below 32 in the first 15 meters.

226

227 ~~During GEOVIDE, diatoms and type 6 haptophytes dominated the bloom close to the IM, while type 6~~
228 ~~haptophytes and dinophytes were dominant in the WEB province (Tonnard et al., in prep.). The IB bloom was~~
229 ~~dominated by type 6 haptophytes and the IrB was dominated by diatoms. GS and NS coastal stations were~~
230 ~~almost exclusively composed of large diatoms. Finally, the LB was dominated by diatoms and type 6 and 8~~
231 ~~haptophytes. The NS, LB, GS and IrB provinces (stations 44 to 77) were sampled just after the bloom peak. The~~
232 ~~LB was characterized by an intense particulate organic carbon (POC) export and high remineralization activity~~

(Lemaitre et al., 2018a). In contrast, low remineralization fluxes and high POC exports were determined within the IB and WEB provinces, where the bloom was still active (Lemaitre et al., 2018a, b).

3.2. Section overview

Total particulate iron (PFe), aluminium (PAI), manganese (PMn) and phosphorus (PP) concentrations spanned a large range of concentrations from below detection to 304, 1544, 21.5, 3.5 and 402 nmol L⁻¹ respectively.

PFe, PAI, and PMn were predominantly found (>90%) in particles larger than 5 µm, except in surface waters, where 20.9% ± 8.6% of PFe, 38.8 ± 8.6% of PP, 35.1 ± 15.4% of PAI and 32.8 ± 16.6% up to 60% of PMn were hosted by smaller particles (0.45-5 µm). The ranges of concentrations are comparable to other studies recently published (Table 2). Data are shown in Figure 3.

3.3. Open Ocean stations :Iberian Abyssal Plain (stations 11 to 17), Western European Basin (stations 19 to 29), Icelandic Basin (stations 32 to 36), Reykjanes Ridge (station 38), Irminger Basin (stations 40 to 60; except Stations 53 and 56) and Labrador Basin (stations 63 to 77)

In the open ocean, particulate iron concentration vertical profiles presented identical patterns at open ocean stations sampled in every oceanic basins encountered along the GEOVIDE section. Median PFe were low at 0.25 nmol L⁻¹ (n=???) within the first 100 m and steadily increased with depth. However, at two stations, elevated concentrations were determined in the upper 100m, up to 4.4 nmol L⁻¹ at station 77 at 40 m and 7 nmol L⁻¹ at station 63 between 70 and 100 m depth. PFe concentrations were increasing gradually increased with depth, with a median PFe of 1.74 nmol L⁻¹ below 1000m (n=???) to reach a maximum close to the bottom. Close to the seafloor of some stations (26, 29, 32, 34, 49, 60, and 71), high concentrations of PFe were observed, up to 88 nmol L⁻¹ (station 71 at 3736 m). These high PFe values were associated with low beam transmissometry value inferior or equal to 97% (Figure 9b and supplementary table S2).

Particulate aluminium (PAI) and manganese (PMn) profiles were similar to PFe profiles, with low median value concentrations were observed measured in the first 100 m (1.88 nmol L⁻¹ (n=??) and 55 pmol L⁻¹ (n=??), respectively) and increased towards the seafloor. Close to the seafloor, high concentrations were determined at the same stations cited above for PFe, with a where high value were observed at certain stations (same than PFe) with maximum of 264 nmol L⁻¹ and 3.5 nmol L⁻¹ for PAI and PMn, respectively at station 71 (supplementary Table S1). Highest particulate phosphorus (PP) concentrations were maximum observed in the first 50m, with a median value of 66 nmol L⁻¹ (n=???). Deeper in the water column, below 200m, PP concentrations decreased to values underbelow 10 nmol L⁻¹ below 200 meters depth. Inter-basins differences were observed within the surface samples, with Irminger basin had the higher median PP concentration being higher in the Irminger Basin (127 nmol L⁻¹, n=???) of the section while the than in the Iberian Abyssal Plain had the lower median (28 nmol L⁻¹), n=???

Finally, above the Reykjanes Ridge, PP, PMn, PAI and PFe concentrations were in the same range than the surrounding open ocean stations. However, close to the seafloor, high concentrations were measured, with PFe, PAI, and PMn reaching 16.2 nmol L⁻¹, 28.8 nmol L⁻¹, and 0.51 nmol L⁻¹ at 1354 m, respectively (Figure 3 and supplementary material Table S1 Table 1, supplementary material and Figure xxx).

270
271 3.4. Margins and Shelves: Iberian Margin (stations 1 to 4), Greenland coast (stations 53, 56
272 and 61) and Newfoundland Shelf (station 78)

273
274 The Iberian margin was characterised by low beam transmissometry values at station 2 (88% at 140 m, Figure
275 9b) suggesting significant particle concentrations. Particulate iron concentrations varied between 0.02 nmol L⁻¹;
276 station 2 to 304 nmol L⁻¹, Station 2. In Within the first 50m, PFe concentrations decreased from the Iberian
277 Shelf (Station 2, 2.53 nmol L⁻¹) towards the shelf break where PFe dropped down from 2.53 nmol L⁻¹ to
278 (station 2, depth) to 0.8 nmol L⁻¹ (Station 1). PFe concentrations increased with depth at all three stations and
279 reached a maximum at the bottom of station 2 (138.5 m) with more than 300 nmol L⁻¹ of PFe. Lithogenic
280 tracers, such as PAI or PMn, presented similar profiles to PFe with concentrations ranging between 0.11 and
281 1544 nmol L⁻¹, and from below detection limit to 2.51 nmol L⁻¹ respectively (station, depth) (Figure 3, Table 1,
282 supplementary material Table S1, Figure xxxxx). Total particulate phosphorus (PP) concentrations were
283 relatively low in surface ranging from undetectable values to 38 nmol L⁻¹ (station xxxxx) (Table 1, supplementary material, Figure
284 xxxxx) in surface; then Maximum PP was measured in surface at Station 1 (20 m depth), then concentrations
285 decreased with depth and were less than 0.7 nmol L⁻¹ below 1000 m depth.
286 Particulate Fe concentrations in In the vicinity of the Greenland shelf, PFe concentrations had a high median
287 concentration value of 10.8 nmol L⁻¹ (n=???) while and were associated with high median PAI and PMn also had
288 high median concentrations of 32.3 nmol L⁻¹ (n=???) and 0.44 nmol L⁻¹ (n=???), respectively. Concentrations of
289 PP were high at the surface with a value of 197 nmol L⁻¹ at 25 m of station 61. Then, PP concentrations
290 decreased strongly, less than 30 nmol L⁻¹, below 100 meters depth. Furthermore, beam transmissometry values
291 in surface waters at these three stations, were the lowest of the entire section, with values below 85 %.
292 Close to the Newfoundland margin, surface waters displayed a small load of particulate trace metals as PFe,
293 PAI, and PMn were below 0.8 nmol L⁻¹, 2 nmol L⁻¹, and 0.15 nmol L⁻¹ respectively. Then close to the bottom of
294 station 78, at 371 m, beam transmissometry values dropped to 94% and were associated with extremely high
295 concentrations of PFe=168 nmol L⁻¹, PAI=559 nmol L⁻¹, and PMn=2 nmol L⁻¹. Total PP concentrations in the
296 first 50 m ranged from 35 to 97 nmol L⁻¹. Below the surface, PP remained relatively high with values up to 16
297 nmol L⁻¹ throughout the water column. (Table 1, supplementary material and Figure XXXX3 and supplementary
298 material Table S1).

299 3.5. Reykjanes Ridge (station 38)

300 Above the Reykjanes Ridge, the upper portion of the Mid Atlantic Ridge, particulate trace
301 elements concentrations were in the same range than the surrounding open ocean stations. However,
302 close to the seafloor, high concentrations were measured on the ridge, with PFe, PAI, and PMn
303 reaching 16.2 nmol L⁻¹, 28.8 nmol L⁻¹, and 0.51 nmol L⁻¹ at 1354 m, respectively. Low concentrations
304 of PP were measured in surface waters, with a median value of 24.8 nmol L⁻¹ in the top 100 m and a
305 maximum of only 72.6 nmol L⁻¹ at 20 m. 3.3. Iberian Margin (stations 1 to 4)

306 The Iberian margin was characterised by low beam transmissometry values at station 2 (88% at 140 m)
307 suggesting significant particle concentrations. Particulate iron concentrations varied between 0.02 nmol L⁻¹ (20
308 m) to 304 nmol L⁻¹ (138 m) in this area. Above the Iberian Shelf, high PFe concentrations were measured in

309 surface (Station 2, 2.53 nmol L⁻¹); then, on the shelf break, surface concentrations dropped down to 0.8 nmol L⁻¹
310 (Station 1 at 20 m depth). PFe concentrations increased with depth at all three stations and reached a maximum
311 at the bottom of station 2 (138.5 m) with more than 300 nmol L⁻¹ of PFe. Lithogenic tracers, such as PAI or
312 PMn, presented similar profiles to PFe with concentrations ranging between 0.11 and 1544 nmol L⁻¹, and from
313 below detection to 2.51 nmol L⁻¹ respectively. The highest concentrations were also measured at the bottom of
314 station 2 (138.5 m). Total particulate phosphorus (PP) concentrations were relatively low in this area ranging
315 from undetectable values to 38 nmol L⁻¹. Maximum PP was measured in surface at Station 1 (20 m depth), then
316 concentrations decreased with depth and were less than 0.7 nmol L⁻¹ below 1000 m depth.

3.4. Iberian Abyssal Plain (stations 11 to 17) and Western European Basin (stations 19 to 29)

320 In the Iberian Abyssal Plain (IAP) and the Western European Basin (WEB), particulate iron concentration
321 vertical profiles were similar (Figure 4); median PFe concentrations were 0.18 nmol L⁻¹ in the first 100 m and
322 steadily increased with depth. Close to the seafloor, concentrations of PFe were up to 1.4 nmol L⁻¹ at every
323 station and reached values superior to 8 nmol L⁻¹ at stations 26 and 29, with low beam transmissometry
324 (<98%). Particulate aluminium profiles matched the PFe profiles, with low median concentrations within the
325 first 100 m of 1.77 nmol L⁻¹ and 26 pmol L⁻¹ respectively. Then, concentrations increased with depth to reach a
326 maximum close to the oceanic floor. At stations 26 and 29, total PAI concentrations reached high values, up to
327 42 nmol L⁻¹. In the Western European Basin, PMn concentrations ranged from below detection to 0.36 nmol L⁻¹,
328 except close to the bottom of stations 26 and 29, where high concentrations of 0.91 and 1.31 nmol L⁻¹ were
329 measured, respectively. Particulate phosphorus profiles, while similar between stations of this basin, differed a
330 lot from the other element profiles. In the WEB, surface median PP concentration was two times higher than in
331 the Iberian margin (60 nmol L⁻¹ against 28 nmol L⁻¹ in the first 50 m with a maximum of 162 nmol L⁻¹ (station
332 21). Concentrations dropped drastically with depth and remained under 10 pmol L⁻¹ below 100 m.

3.5. Icelandic Basin (stations 32 to 36)

336 Concentrations of PFe were in a similar range and displayed analogous profiles to the ones collected in the
337 Western European Basin (figure 4), from below detection to 40.6 nmol L⁻¹; with low values at the surface (<1
338 nmol L⁻¹) and a progressive increase with depth. Close to the basin seafloor, low beam transmissometry (97.4%)
339 measurements were associated with high PFe concentrations of 40.6 nmol L⁻¹ at 3271 m of station 32.
340 Particulate aluminium vertical profiles were similar to those in the WEB but with extremely low surface
341 concentrations below 0.6 nmol L⁻¹; PAI then increased steadily with depth, reaching values up to 2 nmol L⁻¹
342 below 500 m. As previously observed for PFe, PAI concentrations were higher close to the seafloor, from 29
343 nmol L⁻¹ at station 34 to 101 nmol L⁻¹ at station 32. PMn also presented similar distributions than PFe and PAI.
344 Median surface concentrations were low within the first 100 m, 31 pmol L⁻¹ and 35 pmol L⁻¹, respectively, and
345 increased in the deep ocean to reach a maximum of 2.98 nmol L⁻¹ close to the seafloor. The Icelandic Basin had
346 a typical vertical profile for PP, with high concentrations at the surface, reaching 129 nmol L⁻¹ at station 32 and
347 really low concentrations below 150 m, inferior to 20 nmol L⁻¹.

348

349

3.6. Reykjanes Ridge (station 38)

350 Surface concentrations of particulate Fe, Al, and Mn above the Reykjanes Ridge (RR) were similar to the
351 Icelandic Basin (Figure 3). However, close to the seafloor, high concentrations were measured, with PFe, PAl,
352 and PMn reaching 16.2 nmol L^{-1} , 28.8 nmol L^{-1} , and 0.51 nmol L^{-1} at 1354 m, respectively. Low concentrations
353 of PP were measured in surface waters, with a median value of 24.8 nmol L^{-1} in the top 100 m and a maximum
354 of only 72.6 nmol L^{-1} at 20 m.

355

356

3.7. Irminger Basin (stations 40 to 60; except Stations 53 and 56)

357 Particulate Iron, Aluminium and Manganese distributions were similar to stations sampled in the WEB, IeB and
358 IAP provinces (Figure 3). Surface concentrations of these elements were lower than 1.1 nmol L^{-1} , 3.4 nmol L^{-1} ,
359 and 0.4 nmol L^{-1} , respectively. Then, below 50 m depth, concentrations of PFe, PAl, and PMn increased and
360 reached high values close to the seafloor, especially at stations 42 and 44; reaching up to 40 nmol L^{-1} , 90 nmol
361 L^{-1} , and 1.5 nmol L^{-1} respectively. Close to the Greenland margin, at the bottom of stations 49 and 60,
362 concentrations of particulate trace metals were also elevated with PFe greater than 10 nmol L^{-1} . Particulate
363 phosphorus concentrations were relatively high in surface waters, of the Irminger Basin, with a median value of
364 127 nmol L^{-1} within the first 50 m. Particulate phosphorus decreased with depth and remained constant below
365 500 m with concentration below 10 nmol L^{-1} .

366

367

3.8. Greenland coast (stations 53, 56 and 61)

368 Particulate Fe concentrations in the vicinity of the Greenland shelf had a high median concentration of 10.8
369 nmol L^{-1} , while PAl and PMn also had high median concentration of 32.3 nmol L^{-1} and 0.44 nmol L^{-1} ,
370 respectively. Concentrations of PP were maximum at the surface with a value of 197 nmol L^{-1} at 25 m of station
371 61. Then, PP concentrations decreased strongly with depth with values below 30 nmol L^{-1} below 100 meters
372 depth. Furthermore, beam transmissometry values in surface waters at these two stations, were the lowest of the
373 entire section, with values below 85 %.

374

375

3.9. Labrador Basin (stations 63 to 77)

376 In the Labrador Basin, median concentrations of PFe within the first 100 m were low, with a median value of
377 0.9 nmol L^{-1} (n=30). However, at two stations, elevated concentrations were determined, up to 4.4 nmol L^{-1} at
378 station 77 at 40 m and 7 nmol L^{-1} at station 63 between 70 and 100 m depth. Below the surface waters, PFe
379 remained constant with depth until in proximity of the seafloor (Fig. 3). Between stations 64 and 71, the median
380 concentration between 100 m and 200 m above the seafloor was 2.0 nmol L^{-1} (n=39). Particulate Fe
381 concentration at station 63, close to the Greenland margin, remained constant below 100 m depth, with a high
382 median value of 5.7 nmol L^{-1} . On the other side of the Labrador Basin, station 77, close to the Newfoundland
383 margin, constant PFe values of 3 nmol L^{-1} between the surface and 200 m above bottom depth were observed.

384 As previously described, PFe concentration increased close to the seafloor to 88 nmol L⁻¹ at station 71 at 3736
385 m. Particulate Al and Mn displayed similar characteristics to PFe, with low median concentrations at the surface
386 of 3.37 nmol L⁻¹ and 90 pmol L⁻¹ respectively. Close to the seafloor of Station 71, at 3736 m depth, PAl, and
387 PMn reached high concentrations of 264 and 3.5 nmol L⁻¹. Particulate Phosphorus distribution was no different
388 than in the eastern basins, with 71 nmol L⁻¹ median PP within the first 50 m. Then below 50 m, the
389 concentration dropped off quickly to a median PP of 3 nmol L⁻¹.

391 3.10. Newfoundland Shelf (station 78)

392 Close to the Newfoundland margin, surface waters displayed a small load of particulate trace metals as PFe,
393 PAl, and PMn were below 0.8 nmol L⁻¹, 2 nmol L⁻¹, and 0.15 nmol L⁻¹ respectively. Then close to the bottom, at
394 371 m, beam transmissometry values dropped to 94% and were associated with extremely high
395 concentrations of lithogenic elements: PFe=168 nmol L⁻¹, PAl=559 nmol L⁻¹, and PMn=2 nmol L⁻¹. Total PP
396 concentrations in the first 50 m ranged from 35 to 97 nmol L⁻¹. Below the surface, PP remained relatively high
397 with values up to 16 nmol L⁻¹ throughout the water column.

399 4. Discussion

400 Our goal in this work was to investigate mechanisms that drive the distribution of PFe in the North Atlantic, in
401 particular the different routes of supply and removal.

402 Possible candidate sources of PFe include lateral mixing advection offshore from the different margins,
403 atmospheric inputs, recently melted sea ice continental run-off, melting ice shelves and icebergs, resuspended
404 sediments, or hydrothermal inputs and biological pooluptake. Removal processes include remineralization and
405 dissolution processes.

406 In the following sections, we examine each of these sources and processes, explore the evidence for their
407 relative importance, and use compositional data to estimate the particle types and host phases for iron and
408 associated elements.

409 4.1. Analysis of the principal factors controlling variance: near-ubiquitous influence of 410 crustal particles in the water column

411 The positive matrix factorisation Positive Matrix Factorisation (PMF) was run to characterise the main factors
412 influencing the particulate trace elements variances along the GEOVIDE section. In addition to PFe, PAl, PMn,
413 and PP, nine additional elements were included in the PMF: Y, Ba, Pb, Th, Ti, V, Co, Cu and Zn. The analysis
414 has been conducted on samples where all the 13 elements previously cited are above the detection limits; after
415 selection, 445 of the 549 existing data points were used. Analyses were performed using the PMF software,
416 EPA PMF 5.0, developed by the USA Environmental Protection Agency (EPA). Models have been tested with
417 several factors number (from 3 to 6), after full error estimation of each model, we decide to use the
418 configuration providing the lowest errors estimations and in consequence the most reliable. results
419 In consequence, models were set up with four factors and were run 100 times to observe the stability of the
420 obtained results. After displacement, error estimations and bootstraps error estimations, the model was

421 ~~recognised as stable.~~ Results, are shown in Figure 5, indicate the overall variances explained by each of the 5
422 factors.

423 The first factor is characterised by lithogenic elements, representing 86.8% of the variance of PFe, 75.8% of
424 PAI and 90.5% of PTi. The second factor is correlated with both Mn and Pb and explains no less than 76.5%
425 and 77.0% of their respective variances. Ohnemus and Lam (2015) observed this co-relation between
426 manganese and lead particles and explained it by the co-transport on Mn-oxides (Boyle et al., 2005). The
427 formation of barite is causing the third factor constraining 87.7% of the Ba variance in the studied regions.
428 Biogenic barite accumulation within the mesopelagic layer is related to bacterial activity and organic
429 remineralisation (Lemaitre et al., 2018a). A biogenic component is the fourth factor and explained most of
430 particulate phosphorus variance, 83.7%. The micronutrient trace metals, copper, cobalt and zinc, had more than
431 a quarter of their variances influenced by this factor.

432
433
434
435 These results indicate that aAlong the GA01 section, PFe distributions were predominantly controlled by
436 lithogenic material, material and to a smaller extent by remineralisation processes (as seen by a Factor 3
437 contribution of 4.1%). This does not rule out some biogenic influence on PFe distribution, especially in surface,
438 but this contribution is veiled by the high lithogenic contribution. The PMF analysis has been realised on the
439 entire dataset, in consequence, the factors described are highly influenced by the major variations of particulate
440 element concentrations (usually at the interface, i.e. margin, seafloor, surface layer,...).

441 ~~These inputs and processes are discussed below.~~

442 To further investigate the influence of crustal material on the distribution of PFe, it is instructive to examine the
443 distribution of the molar ratio of PFe/PAI along the section as a way to assess the lithogenic inputs (Lannuzel et
444 al., 2014; Ohnemus and Lam, 2015; Planquette et al., 2009) (Figure 6) along the section.

445
446 The PFe/PAI ratio can be used to estimate the proportion of lithogenic particles within the bulk particulate
447 material. A comparison with the Upper Continental Crust (UCC) ratio of Taylor and McLennan (1995), 0.21,
448 was used to calculate the lithogenic components of particles (PFe_{litho}) following Eq. (1):

$$449 \quad \%PFe_{litho} = 100 * \left(\frac{PAI}{PFe} \right)_{sample} * \left(\frac{PFe}{PAI} \right)_{UCC \text{ ratio}} \quad (1)$$

451
452 Then the non-lithogenic PFe is simply obtained using Eq. (2):

$$453 \quad \%PFe_{non_litho} = 100 - \%PFe_{litho} \quad (2)$$

454
455 Both the lithogenic and non-lithogenic fraction of PFe are estimated using in fine the UCC ratio. Spatial and
456 temporal variation of the lithogenic components ratio may falsely influence the estimated fraction value. The
457 PFe_{litho} and $PFe_{excessnon-lithonon-litho}$

Formatted: Space After: 10 pt

459 proxies are interesting tools to evaluate the importance of lithogenic and authigenic formation of Fe
460 oxyhydroxides non-lithogenic (either biogenic or authigenic). Biogenic contributions over the section but have
461 to be used with consideration.

462 Overall, the estimated lithogenic contribution to PFe varies from 25% (station 60, 950 m) to 100% at stations
463 located within the Western European Basin. 100% of estimated lithogenic PFe doesn't necessary mean that
464 biogenic particles are absent; they may just be masked by the important load of lithogenic particles. Important
465 inter-basins variations are observed along the section (Figure 6). The IAP and WEB basins are linked with high
466 median value of the proxy %Fe_{litho}, 90%. This could be linked to a lateral advection of iron rich lithogenic
467 particles sourced from the Iberian margin and to a less extent atmospheric particles with the North Atlantic
468 Central Water flowing northward (Shelley et al., 2017; Garcia-Ibanez et al., 2015). This point is discussed with
469 more detail in section 4.3.1. While the Iceland, Irminger and the Labrador basins are characterised with median
470 %PFe value under 55%. An interesting feature observable was the dramatic decrease of the %PFe proxy values
471 happening at the station 26 (Figure 6). This feature is likely be associated to the presence of the Sub-Arctic
472 Front, located between 49.5 and 51°N latitude and 23.5 and 22°W longitude (Zunino et al., 2017). Indeed, this
473 front which separates cold and fresh water of subpolar origin from warm and salty water of subtropical origin
474 was clearly identifiable at station 26 by the steep gradient of the isotherms and isohalines (Figure 2).

475 Overall, the lithogenic contribution to PFe varies from 24% (station 60, 950 m) to 100% at stations located
476 within the Western European Basin. This could be linked to a lateral advection of iron rich lithogenic particles
477 sourced from the Iberian margin and to a less extent atmospheric particles with the North Atlantic Central Water
478 flowing northward (Shelley et al., 2017; Garcia Ibanez et al. (2015)). This point is discussed with more detail in
479 section 4.3.1.

480 The most striking feature is the almost exclusive lithogenic nature of PFe from stations 1 to 26 throughout the
481 water column, except between 1000 and 3000 m at stations 21 to 26 (Figure 6 and 7). This feature could be
482 linked to the fact that atmospheric inputs generally dominate the supply of PFe—deposited from Saharan dust
483 and transported via the Gulf Stream and North Atlantic Current to the WEB (Shelley et al., 2017; Garcia Ibanez
484 et al. (2015)), even if low atmospheric fluxes were reported during our cruise.

485
486 This feature at 1000 and 2500 m between stations 21 and 26 is likely be associated to the presence of the Sub-
487 Arctic Front, located between 49.5 and 51°N latitude and 23.5 and 22°W longitude (Zunino et al., 2017).
488 Indeed, this front which separates cold and fresh water of subpolar origin from warm and salty water of
489 subtropical origin was clearly identifiable at station 26 by the steep gradient of the isotherms and isohalines. The
490 fact that the WEB was sampled close to but just after the bloom maximum is limiting any higher PFe/PAI
491 signatures (see also section 3.3.4). The intrusion of an old LSW (Garcia Ibanez et al., this issue) at stations 21 to
492 26 between 1000 and 2500 m with a different PFe/PAI signature could explain the smaller contribution of
493 lithogenic PFe in this depth range as atmospheric inputs to the Labrador Sea region are relatively small (Shelley
494 et al., 2017). This is discussed with more detail in section 4.2.

4.2. Fingerpriting watermasses

496 The GEOVIDE section crossed several distinct water masses along the North Atlantic, each of them being
497 distinguishable by their salinity and potential temperature signatures (García-Ibáñez et al., 2015; Figure 2).

498 Based on this study, we applied a Kruskal-Wallis test on molar PFe/PAI ratios of nine water masses (Figure 87)
499 in order to test the presence of significant differences. Water masses for which we had less than 5 data points for
500 PFe/PAI were excluded from this test. As the differences in the median values among the treatment groups were
501 greater than would be expected by chance; the difference in PFe/PAI between water masses is statistically
502 significant ($P = <0.001$).

503 As previously seen, the lithogenic inprint is dominant in the WEB, with MW and NEADW showing PFe/PAI
504 values close to the UCC value of $0.21 \text{ mol mol}^{-1}$. Interestingly, the PFe/PAI signature of $0.36 \text{ mol mol}^{-1}$ within
505 the old LSW_{WEB} is probably due to the effect of biologic inputs associated with the strong bloom encountered in
506 the Irminger Sea than in the WEB (see section 4.3.5).

507 While it appears that lithogenic particles are dominating the water column in the ~~WEB,WEB~~ and that some
508 water masses have a clear PFe/PAI fingerprint, it is important to discuss the origin of these signatures, which is
509 the purpose of the following sections.

510

511 4.3. Tracking the different inputs of particulate iron

512 4.3.1. Inputs at margins: Iberian, Greenland and Newfoundland

513 Inputs from continental shelves and margins have been demonstrated to support high productivity in shallow
514 coastal areas. Inputs of iron from continental margin sediments supporting the high productivity found in
515 shallow coastal regions have been demonstrated in the past (e.g. Cullen et al. (2009), Elrod et al. (2004), Jeandel
516 et al. (2011), Ussher et al. (2007)) and sometimes, were shown to be advected at great distances from the coast
517 (e.g. Lam et al., 2008). ~~Moreover, freshwater inputs that are usually present in these regions can also play a key~~
518 ~~role in the global biogeochemical cycling of trace metals (Blain and Tagliabue, 2016; Guieu et al., 1991; Martin~~
519 ~~and Meybeck, 1979). Rivers, runoff and continental glacial melt and/or sea ice melt can also supply dissolved~~
520 ~~and particulate iron to coastal waters, thus sustaining important phytoplankton production (Fung, 2000).~~

521 In the following section, we will investigate these possible candidate sources in proximity of the different
522 margins encountered. Along the GEOVIDE section, sediments at margins were of various compositions
523 (Dutkiewicz et al., 2015). Sediments originating from the Iberian margin were mainly constituted of silts and
524 clays (Cacador et al., 1996; Duarte et al., 2014). East Greenland margin sediments were a mixture of sands and
525 grey/green muds, while, sediments from the West Greenland margin were mainly composed of grey/green muds
526 (Loring and Asmund, 1996). At the western end of the section, sediments from the Newfoundland margin were
527 composed of gravelly and sandy muds (Mudie et al., 1984). The different sediment compositions of the three
528 margins sampled during GEOVIDE have different mineralogy/composition, which are reflected in their
529 different PFe/PAI ratios (Figure 89). While the Iberian Margin had a PFe/PAI close to UCC ratio, ~~mainly due to~~
530 ~~seasonal dust inputs from North Africa,(Shelley et al., 2017),~~ the highest biogenic contribution ratio could be
531 seen at the East Greenland (stations 53 and 56) and West Greenland (station 61) Margins, with median PFe/PAI

532 reaching 0.45 mol mol⁻¹. The Newfoundland margin displayed an intermediate behaviour, with Fe/Al ratios of
533 0.35 mol mol⁻¹.

534

535

536 In addition to PAI, PMn can be used as a tracer of inputs from shelf resuspension (Lam and Bishop, 2008).
537 Indeed, Mn is really sensitive to oxidation mediated by bacteria (Tebo et al., 1984; Tebo and Emerson, 1985)
538 and forms manganese oxides (MnO₂). These authigenic particles lead to an enrichment of Mn in particle
539 compositions. In order to track the influence of shelf resuspension, a percentage of sedimentary inputs “%bulk
540 sediment inputs” can be ~~calculated~~ estimated using PMn/PAI ratio from GEOVIDE samples and the PMn/PAI
541 UCC value (0.0034; Taylor and McLennan, 1995) according to the following equation:

$$542 \quad \% \text{bulk sediment PMn} = 100 * \left(\frac{\text{PAI}}{\text{PMn}} \right)_{\text{sample}} * \left(\frac{\text{PMn}}{\text{PAI}} \right)_{\text{UCC ratio}} \quad (3)$$

543 This proxy is a good indicator of direct and recent sediment resuspension. We assume that particles newly
544 resuspended in water column will have the same PMn/PAI ratio than the UCC ratio leading to a “%bulk
545 sediment Mn” of 100%. ~~This value will decrease by authigenic formation of Mn oxides. This proxy assumes~~
546 ~~homogeneity of the sediment PMn/PAI ratio through the section which is maybe not completely the case at~~
547 ~~every station. In consequence, this proxy is only a tool to identify new benthic resuspension at specific location~~
548 ~~and inter-comparison between several locations is not possible.~~—When a sample presents a “%bulk sediment
549 Mn” greater than 100%, we assign a value of 100% to simplify the following discussion.—As the Mn cycle can
550 also be affected by biologic uptake (e.g. Peers and Price, 2004; Sunda and Huntsman, 1983), this proxy is only
551 used at depths where biologic activity is negligible (i.e. below 150m depth).

552

553 *The Iberian margin*

554 Coastal waters of the Iberian Shelf are impacted by the runoff for the Tagus River, which is characterised by
555 high suspended matter discharges, ranging between 0.4 to 1 × 10⁶ tons yr⁻¹, and with a high anthropogenic
556 signature (Jouanneau et al., 1998). During the GEOVIDE section, the freshwater input was observable at
557 stations 1, 2 and 4 in the first 20 m; salinity was below 35.2 psu while surrounding waters masses had salinity
558 up to 35.7 psu. Within the freshwater plume, particulate concentrations were important at station 2, ~~with at 20m,~~
559 PFe ~~was of~~ 1.83 nmol L⁻¹. Further away from the coast, the particulate concentrations remained low at 20m
560 depth, with PFe, PAI, and PMn concentrations of 0.77 nmol L⁻¹, 3.5 nmol L⁻¹, and 0.04 nmol L⁻¹, respectively at
561 station 1. The low expansion of the Tagus plume is likely due to the rapid settling of suspended matter. Indeed,
562 our coastal station 2 was already located at around 50 km of the Iberian coast and according to Jouanneau et al.
563 (1998), the surface particle load can be observable at a maximum 30km of the Tagus estuary.

564 Besides, ADCP data acquired during GEOVIDE (Zunino et al., 2017) and several studies have reported an
565 intense current spreading northward coming from Strait of Gibraltar and Mediterranean Sea, leading to a strong
566 resuspension of benthic sediments above the Iberian Shelf, e.g. Biscaye and Eittrheim (1977), Eittrheim et al.
567 (1976), McCave and Hall (2002), Spinrad et al. (1983). The importance of the sediment resuspension was
568 observable by low beam transmissometry value (87.6%) at the bottom of station 2. This important sediment
569 resuspension led to an extensive input of lithogenic particles within the water column associated with high

570 concentrations of PFe (304 nmol L⁻¹), PAI (1500 nmol L⁻¹), and PMn (2.5 nmol L⁻¹) (Figure 3, Table S1).
571 Moreover, one hundred percent of PFe is estimated to have a lithogenic origin (Figure 4+10) while 100% of the
572 PMn was ~~estimated to be~~ the result of a recent sediment resuspension according to the %Fe_{litho} and “%bulk
573 sediment Mn” proxies (supplementary material, Table S+S2), confirming the resuspended particle input.

574 At distance from the shelf, within the Iberian Abyssal Plain, an important lateral advection of PFe from the
575 margin was observable (Figure 4+10). These lateral inputs occurred at two depth ranges: between 400 and 1000
576 m ~~at~~ seen at stations 4 and 1, with PFe concentrations reaching 4 nmol L⁻¹, and between 2500 m and the bottom
577 (3575 m) of station 1, with PFe concentrations reaching 3.5 nmol L⁻¹. While 100% of PFe had a lithogenic
578 ~~origin~~signature, the sedimentary source input ~~estimation~~ decreased, between 40% and ~~85~~90% of the PMn
579 (Figure 4+10). Transport of lithogenic particles was observable until station 11 (12.2°W) at 2500 m where PFe
580 concentration was 7.74 nmol L⁻¹ and 60% of PMn had a sedimentary origin (Figure 9+10). Noteworthy, no
581 particular increase in PFe, PMn or PAI was seen between 500 and 2000 m depth, where the MOW spreads,
582 which is consistent with that was observed DFe concentrations (Tonnard et al., this issue); ~~it is~~ yet in contrast with
583 the dissolved aluminium values (Menzel Barraqueta et al, subm., this issue) which were high in the MOW and
584 with the study of Ohnemus and Lam (2015) that reported a maximum PFe concentration at 695 m depth
585 associated with the particle-rich Mediterranean Overflow Water (Eitrem et al., 1976) in the IAP. However,
586 their station was located further south of our station 1. The shallower inputs observed at stations 1 and 4 could
587 therefore be attributed to sediment resuspension from the Iberian margin and nepheloid layer at depth for station
588 1.

589 Therefore, the Iberian margin appears to be an important source of lithogenic-derived iron-rich particles in the
590 Atlantic Ocean; shelf resuspension impact was perceptible until 280 km away from the margin (Station 11) in
591 the Iberian Abyssal Plain.

592

593 *South Greenland*

594 Several studies already demonstrated the importance of icebergs and sea ice as source of dissolved and
595 particulate iron (e.g. van der Merwe et al., 2011a, 2011b; Planquette et al., 2011; Raiswell et al., 2008). The
596 Greenland shelf is highly affected by external fresh water inputs as ice-melting or riverine runoff (Fragoso et al.,
597 2016), that are important sources of iron to the Greenland Shelf (Bhatia et al., 2013; Hawkings et al., 2014;
598 Statham et al., 2008).

599 Both East and West Greenland shelves (stations 53 and 60) had high concentration of particles (beam
600 transmissometry of 83%) and particulate trace elements, reaching 22.1 nmol L⁻¹ and 18.7 nmol L⁻¹ of PFe,
601 respectively (station 53 at 100m and station 61 at 136 m). During the cruise, the relative freshwater observed
602 (S<33 psu) within the first 25 meters of stations 53 and 61 were associated with high PFe (19 nmol L⁻¹), PAI (61
603 nmol L⁻¹), PMn (0.6 nmol L⁻¹) and a low beam transmissometry (≤ 85%) (Figure 4+9 and Table S1). Particles
604 associated were enriched in iron compared to aluminium, as PFe/PAI ratio was 0.3 within the meteoric water
605 plume. High biological production, in agreement with PP concentrations reaching 197 nmol L⁻¹ induced by the
606 supply of bioavailable dissolved iron from meteoric water (Raiswell et al., 2008; Statham et al., 2008.; Tonnard
607 et al., submitted, this issue), ~~lead~~ed to a transfer of DFe to the particulate phase. This is in line with the fact that
608 around 30% ~~of the~~ PFe had a non-lithogenic ~~and likely biogenic~~ origin. In addition, only ~~35%~~40% ~~of the~~ PMn
609 originated from resuspended sediments. Interestingly, these two proxies remained constant from the seafloor to

610 the surface (Station 49, Figure 4410), with around 25% of the PMn of sedimentary origin, which could be due to
611 an important mixing happening on the shelf. The lithogenic PFe could result from the release of PFe from
612 Greenland bedrock captured during the ice sheet formation on land.

613 The spatial extent of the off-shelf lateral transport of particles was not important on the east Greenland coast.
614 Indeed, no visible increase of particulate trace metal concentrations was visible at the first station off-shelf,
615 station 60 (Figure 4410), except at 1000 m depth, where a strong increase (up to 8990%) of sedimentary PMn
616 was seen. This is probably due to the East Greenland Coastal Current (EGCC) that was located at station 53
617 constrained these inputs while stations 56 and 60 were under the influence of another strong current, the East
618 Greenland-Irminger current (EGIC) (Zunino et al., 2017).

619
620 To the west of the Greenland margin, lateral transport of particles was slightly more important. Noticeable
621 concentrations of particulate lithogenic elements were observable until station 64 located 125 km away from
622 shoreline. These particles had decreasing PFe lithogenic contribution (520%) with a similar (257%) sedimentary
623 PMn content than closer to the margin. The increasing nature of non-lithogenic PFe is linked to the bloom in
624 surface (associated with a PFe/PAI ratio of 0.30 mol mol⁻¹, and a PP of 197 nmol L⁻¹ at station 61 and a Chl-a
625 concentrations of 6.21 mg m⁻³), with the biogenic PFe settling down along the transport of particles.

626
627 Therefore, particles newly resuspended from Greenland sediments are an important source, representing around
628 a third of the pMn pool, combined with surface inputs such as riverine runoff and/or ice-melting that are
629 delivering particles on the shelf and biological production. Unlike the Iberian shelf, Greenland margin was not
630 an important provider of particulate metals inside the Irminger and Labrador Basin, due to the circulation that
631 constrained the extent of the margin plume.

632 633 *The Newfoundland Shelf*

634 Previous studies already described the influence of fresh water on the Newfoundland shelf from the Hudson
635 Strait and/or Canadian Arctic Archipelago (Fragoso et al., 2016; Yashayaev, 2007). Yashayaev (2007) also
636 monitored strong resuspension of sediments associated with the spreading of Labrador Current along the West
637 Labrador margin.

638 Close to the Newfoundland coastline, at station 78, high fresh water discharge (≤ 32 psu) was observed in
639 surface (Benetti et al., 2017). Interestingly, these freshwater signatures were not associated with elevated
640 particulate trace metal concentrations. Distance of meteoric water sources implied a long travel time for the
641 water to spread through the Labrador Basin to our sampling stations. Along the journey, particles present
642 originally may have been removed from water column by gravitational settling.

643 The proportion of lithogenic PFe was relatively high and constant in the entire water column, with a median
644 value of 67-70%. At station 78, 95100% of the PMn had a sedimentary origin close to the seafloor (371 m). The
645 spreading of the recent sediment resuspension was observable until 140 m depth where the contribution of
646 sedimentary Mn was still 51% (Figure 4410, Table S2). This could correspond to an intense nepheloid layer as
647 previously reported by Biscaye and Eittrheim (1977) (see also section 3.3.2). The high PFe concentration (184
648 nmol L⁻¹, station 78, 371 m) associated with a high percentage of sedimentary PMn (95%) observed at the

Formatted: Space After: 0 pt

649 bottom of this station, was therefore the result of an important resuspension of shelf sediments. This was
650 confirmed with low transmissometry values of 95%.

651 ~~Despite the~~ important phytoplanktonic community present (~~maximum Chl-a= 4.91 mg m⁻³~~, Tonnard et al., in
652 prep), ~~is linked to the low PFe remained low of at~~ 0.79 nmol L⁻¹ at 10 m, but, ~~with the~~ high PFe/PAI ratio, up to
653 0.4, and ~~the~~ PP concentration of 97 nmol L⁻¹, ~~confirming~~ the biologic influence. Either the biogenic particles
654 settled quickly, and/or they were quickly remineralized. Concerning this latter process, intense remineralization
655 ~~at station 77 (7 mmol C m⁻² d⁻¹ compared to 4 mmol C m⁻² d⁻¹ in the Western European Basin) at station 77~~ has
656 been reported by Lemaitre et al. (2018a ~~and 2018b~~), which could explain the low PFe values throughout the
657 water column.

658 ~~That said, resuspended particles are were still laterally transported off shelf until station 71 (Figure 6) where~~
659 ~~PFe concentrations were higher than the background value, up to 2 nmol L⁻¹ at depths greater than 100 m.~~

660

661 Along the GEOVIDE section, continental shelves provided an important load of particles within the surrounding
662 water column. The three margins sampled during GEOVIDE behaved differently; the Iberian margin discharged
663 high quantities of lithogenic particles far away from the coast while the Greenland and Newfoundland margins
664 did not reveal important PFe concentrations. Spreading of particles is tightly linked to hydrodynamic conditions,
665 which in the case of the Greenland margin, prevented long distance seeding of PFe. Moreover, each margin
666 showed a specific PFe/PAI ratio (Figure 89) indicating different composition of the resuspended particles.
667 Resuspended particles represent the composition of sediment at the margin if oxido-reductive transformation of
668 iron and aluminium are considered negligible under these circumstances. Differences between margins were due
669 to the presence of non-crustal particles, ~~either biogenic or authigenic~~. Biological production in surface waters
670 ~~and authigenic formation of iron hydroxide~~ produces particles with a higher PFe/PAI content and their export
671 through the water column to the sediment increased the PFe/PAI ratio at depth. Regions where biological
672 production is intense such as in the vicinity of Newfoundland presented higher PFe/PAI ratios of resuspended
673 benthic particles. ~~These results are in agreement with the study of Lam et al. (2017), which showed the different~~
674 ~~behaviour between margins are a function of several parameters such as boundary currents, internal waves and~~
675 ~~margin sediment composition.~~

676

677

4.3.2 Benthic resuspended sediments

678 Benthic nepheloid layers (BNLs) ~~(BNLs) can play a significative role in trace element distributions at depth as~~
679 ~~previously described (Dutay et al., 2015; Lam et al., 2015; Ohnemus et al., 2015; Revels et al., 2015).~~ BNLs are
680 important layers where local resuspension of sedimentary particles (Bishop and Biscaye, 1982; Eittréim et al.,
681 1976; Rutgers Van Der Loeff et al., 2002) occur due to strong hydrographic stresses (~~i.e. boundary currents,~~
682 ~~benthic storms and deep eddies~~) interacting with the ocean floor (~~(Biscaye and Eittréim, 1977; Eittréim et al.,~~
683 ~~1976; Gardner et al., 2017, 2018).~~ ~~In the North Atlantic, boundary currents were suspected to be the origin of~~
684 ~~theses stresses (Biscaye and Eittréim, 1977; Eittréim et al., 1976) but more recent studies demonstrate the~~
685 ~~essential role of benthic storms and deep eddies (Gardner et al., 2018).~~ Along the GA01 section, BNLs were
686 observable in each province with different strengths (Figures 3 and 12).

687

688 In BNLs located within the WEB, PFe concentrations reached up to 10 nmol L⁻¹ (stations 26 and 29, [Table S1](#),
689 [supplementary material](#)). These concentrations were smaller than PFe concentrations encountered in BNL from
690 the Icelandic, Irminger and Labrador Basins, where benthic resuspension led to PFe concentrations higher than
691 40 nmol L⁻¹, even reaching 89 nmol L⁻¹ at the bottom of station 71 (3736 m). Moreover, in the Irminger and
692 Labrador Basins, PFe/PAI molar ratios within BNLs were higher than the ones measured within the WEB at
693 station 26 and 29. In the Irminger Basin, PFe/PAI reached 0.4 mol mol⁻¹, which could reveal a mixture of
694 lithogenic and biogenic matter previously exported. This feature was also observed in the Labrador Basin, with
695 PFe/PAI ratio ranging between 0.34 and 0.44 mol mol⁻¹. In contrast, BNLs sampled in the WEB have clearly a
696 lithogenic imprint, with PFe/PAI molar ratios close to the crustal one. Resuspended sediments with a non-crustal
697 contribution seem to hold a higher PFe content than sediments with a lithogenic characteristic. Nevertheless,
698 interestingly all BNLs present during GEOVIDE were spreading identically, with impacts observable up to 200
699 meters above the oceanic seafloor (Figure 112), as reflected in beam transmissometry values, and PFe
700 concentrations, that returned to a background level at 200 m above the seafloor. The presence of these BNLs has
701 also been reported by Le Roy et al. (submitted, this issue). Important differences of PFe intensities could also be
702 due to different hydrographic components and topographic characteristics. As previously explained, two main
703 triggers of BNLs are benthic storms and deep eddies; by definition these processes are highly variable
704 geographically and temporally, but no physical data could allow us to investigate further this hypothesis.
705 Along the GEOVIDE section, BNLs are providing high concentrations of particulate trace element in the deep
706 open ocean, contributing highly to the total trace elements budget as iron. ~~Important differences of PFe~~
707 ~~intensities could also be due to different hydrographic components and topographic characteristics. As~~
708 ~~previously explained, two main triggers of BNLs are benthic storms and deep eddies; by definition these~~
709 ~~processes are highly variable geographically and temporally, but no physical data could allow us to investigate~~
710 ~~further this hypothesis.~~

711
712

4.3.3. Reykjanes Ridge inputs

713 ~~Recently, hydrothermal inputs of iron in the open ocean have been re-evaluated by (Fitzsimmons et al., 2017;~~
714 ~~Resing et al., 2015; Tagliabue et al., 2014). These studies demonstrated the importance of hydrothermal~~
715 ~~activities on the global iron biogeochemical cycle through particulate and dissolved iron fluxes. During the~~
716 ~~cruise, samples of station 38 have been collected above the Reykjanes Ridge, the upper section of the Mid-~~
717 ~~Atlantic Ridge in the North Atlantic, which has inferred hydrothermal sites from several studies conducted in~~
718 ~~the area (Baker and German, 2004). Above the ridge, high PFe concentrations were measured, reaching 16 nmol~~
719 ~~L⁻¹ just above the seafloor, while increased DFe concentrations were reported to the East of the ridge (Tonnard~~
720 ~~et al., this issue). The exact sources of iron-rich particles cannot be well constrained, as they could come from~~
721 ~~active hydrothermal vents or resuspension of particulate matter from new crustal matter produced at the ridge.~~
722 According to the oceanic circulation (Zunino et al., 2017; Garcia-Ibanez et al., 2017), hydrothermal particles
723 could have been seen in the ISOW within the Icelandic Basin. Nevertheless, at the vicinity of the ridge, scanning
724 electron microscope (SEM) analyses of our samples did reveal a number of biological debris and clays but not
725 the presence of iron (oxy)-hydroxide particles, which are known to be highly produced close to hydrothermal
726 vents (Elderfield and Schultz, 1996). Their absence could thus indicate an absence of vents. However, other

727 proxies, such as helium-3, are necessary to claim with more accuracy the presence or absence of an
728 hydrothermal source close to station 38.

729
730 ~~Alternatively, resuspended sediments transported with ISOW flowing across the Reykjanes Ridge could explain~~
731 ~~the high PFe concentrations below 1000 m depth at station 38. This feature was associated with lower median~~
732 ~~PFe concentrations and PFe/PAI ratios (Figure 7) at station 40 (2.2 nmol L⁻¹, and 0.58 mol mol⁻¹ respectively)~~
733 ~~than at station 38 (6.8 nmol L⁻¹, 0.48 mol mol⁻¹ respectively). Moreover, PMn had a 19% sedimentary origin,~~
734 ~~constant from the bottom to 1163 m depth, a contribution that is very low for the shallower water depths.~~
735 ~~Consequently, the increase in PFe within the ISOW_{west} more likely came from sediment resuspension as the~~
736 ~~ISOW_{west} flows through the Charlie Gibbs Bight Fracture Zones.~~

737 738 4.3.4. Atmospheric inputs

739 Atmospheric deposition is an important input of trace elements in surface of the open ocean (e.g. (Jickells et al.,
740 2005). Atmospheric inputs, both wet and dry, were reported to be low during the GEOVIDE cruise (Menzel-
741 barraqueta et al., 2018, this issue; Shelley et al., 2017; 2018). In fact, oceanic particles measurements in surface
742 waters along the section did not reveal high PFe or PAI concentrations, therefore, the surface composition of
743 particles did not seem to be highly affected by atmospheric deposition at the time of the cruise. ~~However,~~
744 ~~PFe/PAI ratio was closed to the UCC one, probably due to the overall influence of atmospheric deposition in~~
745 ~~this area.~~ One pattern is also interesting to note: the surface waters of the Iberian Abyssal Plain and Western
746 European Basin, between stations 11 and 23 presented a characteristic feature with really low PFe/PAI
747 elemental ratios, of 0.11, smaller than the UCC ratio of 0.21 (Figure 6). Such low ratios have been reported in
748 the same region by Barrett et al. (2012). One possible explanation is given by Buck et al. (2010) who described
749 Fe-depleted aerosols in this area of the North Atlantic with PFe/PAI ratio below UCC ratio. However, Shelley et
750 al. (2017) found a higher PFe/PAI ratio around 0.25 in this area (their sample geoa5-6). This result, highlights
751 some of the difficulties that link atmospheric inputs to water column data (Baker et al., 2016), and implies a
752 probable fractionation after aerosol deposition. In addition, there is high spatial and temporal variability of
753 atmospheric deposition (Mahowald et al., 2005) and a certain degree of uncertainty about the dissolution
754 processes of atmospherically-transported particles (Bonnet and Guieu, 2004).

755 756 4.3.5. Influence of phytoplankton assemblages, remineralisation and scavenging in 757 the upper water column

758 ~~Biological activity in surface waters impacts the particle composition in the upper water column. In bulk particle~~
759 ~~samples, direct measurement of the biogenic metal fraction is not possible due to the heterogeneity of particles,~~
760 ~~and in particular, the presence of lithogenic particles (Collier and Edmond, 1984). It is however possible to~~
761 ~~estimate the $\frac{PFe_{nonlitho}}{PFe_{excess}}/PP$ molar ratios, based on Eq. (1) and (23), and assuming that most of the PP is of~~
762 ~~biogenic origin. As 100% of the PFe was estimated to be of lithogenic origin, stations 1 to 26 are excluded from~~
763 ~~the discussion below. Overall, the median $\frac{PFe_{excess}}{PP}$ molar ratios varied from 1.0 (Irminger Basin) to 38.7~~
764 ~~mmol mol⁻¹ (Greenland margin) in the upper 50 m. These ratios are consistent with the few available bulk~~

765 PFe/PP ratios available in the literature (Twining and Baines, 2013 and references therein), ranging from 1 to 31
766 mmol mol⁻¹ and the phytoplankton assemblages encountered during GEOVIDE (Tonnard et al., in prep.). This
767 corresponds to a % PFe_{bio} of x to x% in the upper 50m. Interestingly, the biogenic contribution is higher in the
768 basin than in the basin.

769 Overall, the median PFe_{nonlitho}/PP molar ratios varied from 1.0 (Irminger Basin) to 38.7 mmol mol⁻¹ (Greenland
770 margin) in the upper 50 m. These ratios are consistent with the few available bulk PFe/PP ratios available in the
771 literature (Twining and Baines, 2013 and references therein), ranging from 1 to 31 mmol mol⁻¹ and the
772 phytoplankton assemblages encountered during GEOVIDE (Tonnard et al., in prep.). Indeed, the highest
773 PFe_{nonlitho}/PP molar ratio determined at stations 53 and 56 close to the South Greenland margin coincide
774 with a bloom mostly composed of large diatoms, whereas, the smallest ratios were associated with a bloom
775 mainly composed of cyanobacteria and haptophytes (Tonnard et al., in prep.). The effect of biological uptake is
776 also clearly visible when looking at PFe/PAI vertical variation, which increases from the surface to
777 approximately 100m depth (Figure 13), except in the Iberian Margin, which is under the strong influence of
778 lithogenic inputs.

781 At deeper depths, pelagic remineralisation processes influence the composition of particles (Barbeau et al.,
782 1996, 2001; Boyd et al., 2010; Strzpek et al., 2005). Taking in account remineralization depths that are derived
783 from Baxs proxy which is described and discussed in great detail in Lemaitre et al. (this issue), it is possible to
784 look at the vertical variation of PFe_{bio}/PP along the section (Figure 13).

785 Close to the IM and within the IAP, no PFe/PAI decrease that could point to a preferential remineralisation of
786 PFe over PAI could be observed within the remineralisation depth (200 to 400 m depth, Figure 13), whereas
787 preferential remineralisation of PP over PFe occurs, as reflected by increasing PFe/PP ratios (Figure 14). This is
788 probably due to the fact that remineralisation rates were low (Lemaitre et al., 2018a), and that PFe was mostly of
789 lithogenic origin, more difficult and slow to remineralize (Boyd et al., 2010). Below 600 m depth, scavenging
790 processes could explain the increasing PFe:PP ratios, from 0.30 to 0.80 mol mol⁻¹ at station 13, which is
791 consistent with decreasing dFe concentrations within this depth range reported in Tonnard et al. (this issue).

792 Within the WEB, between 200 and 500 m depth, remineralisation of PFe over PAI occurs, although reported to
793 be small (Lemaitre et al., 2018a) as reflected by decreasing PFe:PAI ratios (Figure 13), while PFe:PP ratios
794 remained constant, pointing out to similar remineralisation rates of PFe and PP. Below 600 m depth, a stronger
795 scavenging of DFe onto particles formation of Fe oxyhydroxydes (si tu peux calculer et reporter les % à ces
796 intervalles de profondeur, ça aiderait) than in IM and IAP is likely to explain the increasing ratios of PFe:PAI
797 from 0.18 to 0.30 mol mol⁻¹ and PFe:PP from 0.047 to 0.367 (Station 21), and from 0.16 to 1.05 (Station 26) mol
798 mol⁻¹. Similar patterns occur in IcB (station 32), as dFe concentrations increased (Tonnard et al., this issue)
799 therefore ruling out the possibility of PFe enrichment from scavenging.

801 Above the RR, and in the IrB, at station 38, PFe_P is remineralized preferentially over PAI and PFe_o, with
802 decreasing increasing PFe:PAI ratios from 0.46 to 0.19 mol mol⁻¹ and decreasing PFe:PP ratios from 0.24 to
803 0.04 mol mol⁻¹. This interesting ese features is are associated with moderate and high POC remineralisation

804 fluxes (Lemaitre et al., 2018a) at stations 38 and 44 respectively (Figure 13), and the fact that a stronger fraction
805 of PFe was associated with biogenic lithogenic material ($PFe_{bio} = \%$, $PFe_{litho} = \%$), easier to recycle.

806 In the IrB, PP is preferentially remineralized over PFe and PAI, as reflected by increasing PFe:PP ratios and
807 constant PFe:PAI ratios within the remineralisation depth. This is associated with high POC remineralisation
808 fluxes (Lemaitre et al., 2018a) and a high proportion of lithogenic PFe.

809 Finally, within the LB, PFe:PAI and PFe:PP remained constant within the deep remineralisation depth,
810 extending from 200 to 1000 m depth due to the deep convection of the LSW (Lemaitre et al., 2018a). In this
811 basin, either PP and PFe are remineralized at a constant rates, but the fact that dFe is depleted (Tonnard et al.,
812 this issue) in this depth range points out to the influence of scavenging. Below 1000 m, PFe:PP ratios increase
813 from 0.29 to 0.85 mol mol⁻¹, while PFe:PAI ratios still remain constant. This could be explained by the fact that
814 most PP has been recycled due to the strongest remineralisation fluxes reported in this area (Lemaitre et al.,
815 2018a).

816 5. Conclusions

817 This investigation of the PFe compositions of suspended particulate matter in the North Atlantic indicates the
818 pervasive influence of crustal particles, augmented by sedimentary inputs at margins, and at depths, within
819 benthic nepheloid layers.

820 Indeed, along the GEOVIDE section, continental shelves provided an important load of particles within the
821 surrounding water column, with PFe mostly residing in non-biogenic particulate form. The Iberian margin
822 discharged high quantities of lithogenic particles originating from riverine inputs far away from the coast while
823 the Greenland margin did not reveal a long distance seeding of PFe, due to hydrodynamic conditions. Both
824 Greenland and Newfoundland margins PFe resuspended particles were under a strong biogenic influence that
825 were exported at depth. This resulted in different remineralisation fluxes among the different provinces.
826 Scavenging processes could also be visible at depths greater than 1000 m, these effects being the most
827 pronounced within the WEB Labrador Basin.

828 Finally, resuspended sediments above the Reykjanes Ridge increased the PFe composition of the Iceland
829 Scottish Overflow Water. A similar feature occurs for the Labrador Sea Water, as it flows from the Irminger
830 Basin to the Western European Basin.

835 Acknowledgments

836 We are greatly indebted to the captain and crew of the N/O Pourquoi Pas? for their help during the GEOVIDE
837 mission and clean rosette deployment. We would like to give special thanks to Fabien Pérault and Emmanuel de
838 Saint Léger for their technical expertise, to Catherine Schmechtig for the GEOVIDE database management and
839 Greg Cutter for his guidance in setting up the new French clean sampling system. We also would like to thanks
840 Reiner Schlitzer for the Ocean Data View software (ODV).

841 This work was supported by the French National Research Agency (ANR-13-BS06-0014, ANR-12-PDOC-
842 0025-01), the French National Centre for Scientific Research (CNRS-LEFE-CYBER), the LabexMER (ANR-
843 10-LABX-19), and Ifremer. It was supported for the logistic by DT-INSU and GENAVIR.

844

845 **References**

846

847 Aguilar-Islas, A. M., Rember, R., Nishino, S., Kikuchi, T. and Itoh, M.: Partitioning and lateral transport of iron
848 to the Canada Basin, *Polar Sci.*, 7(2), 82–99, doi:10.1016/j.polar.2012.11.001, 2013.

849 Baker, A. R., Adams, C., Bell, T. G., Jickells, T. D. and Ganzeveld, L.: Estimation of atmospheric nutrient
850 inputs to the Atlantic Ocean from 50°N to 50°S based on large-scale field sampling: Iron and other dust-
851 associated elements, *Global Biogeochem. Cycles*, 27(3), 755–767, doi:10.1002/gbc.20062, 2013.

852 Baker, A. R., Landing, W. M., Bucciarelli, E., Cheize, M., Fietz, S., Hayes, C. T., Kadko, D., Morton, P. L.,
853 Rogan, N., Sarthou, G., Shelley, R. U., Shi, Z., Shiller, A. and van Hulten, M. M. P.: Trace element and isotope
854 deposition across the air–sea interface: progress and research needs, *Philos. Trans. R. Soc. A Math. Phys. Eng.*
855 *Sci.*, 374(2081), 20160190, doi:10.1098/rsta.2016.0190, 2016.

856 [Barbeau, K., Moffett, J. W., Caron, D. A., Croot, P. L. and Erdner, D. L.: Role of protozoan grazing in relieving
857 iron limitation of phytoplankton, *Nature*, 380\(6569\), 61–64, doi:10.1038/380061a0, 1996.](#)

858 [Barbeau, K., Kujawinski, E. B. and Moffett, J. W.: Remineralization and recycling of iron, thorium and organic
859 carbon by heterotrophic marine protists in culture, *Aquat. Microb. Ecol.*, 24\(1\), 69–81, doi:10.3354/ame024069,
860 2001.](#)

861 Barrett, P. M., Resing, J. A., Buck, N. J., Buck, C. S., Landing, W. M. and Measures, C. I.: The trace element
862 composition of suspended particulate matter in the upper 1000m of the eastern North Atlantic Ocean: A16N,
863 *Mar. Chem.*, 142–144, 41–53, doi:10.1016/j.marchem.2012.07.006, 2012.

864 Berger, C. J. M., Lippiatt, S. M., Lawrence, M. G. and Bruland, K. W.: Application of a chemical leach
865 technique for estimating labile particulate aluminum, iron, and manganese in the Columbia River plume and
866 coastal waters off Oregon and Washington, *J. Geophys. Res.*, 113, C00B01, doi:10.1029/2007JC004703, 2008.

867 Bergquist, B. A., Wu, J. and Boyle, E. A.: Variability in oceanic dissolved iron is dominated by the colloidal
868 fraction, *Geochim. Cosmochim. Acta*, 71(12), 2960–2974, doi:10.1016/j.gca.2007.03.013, 2007.

869 Bhatia, M. P., Kujawinski, E. B., Das, S. B., Breier, C. F., Henderson, P. B. and Charette, M. A.: Greenland
870 meltwater as a significant and potentially bioavailable source of iron to the ocean, *Nat. Geosci.*, 6(4), 274–278,
871 doi:10.1038/ngeo1746, 2013.

872 Biscaye, P. E. and Eitrem, S. L.: Suspended Particulate Loads and Transports in the Nepheloid Layer of the
873 Abyssal Atlantic Ocean, *Dev. Sedimentol.*, 23(C), 155–172, doi:10.1016/S0070-4571(08)70556-9, 1977.

874 Bishop, J. K. B. and Biscaye, P. E.: Chemical characterization of individual particles from the nepheloid layer in
875 the Atlantic Ocean, *Earth Planet. Sci. Lett.*, 58(2), 265–275, doi:10.1016/0012-821X(82)90199-6, 1982.

876 Bishop, J. K. B. and Fleisher, M. Q.: Particulate manganese dynamics in Gulf Stream warm-core rings and
877 surrounding waters of the N.W. Atlantic, *Geochim. Cosmochim. Acta*, 51(10), 2807–2825, doi:10.1016/0016-
878 7037(87)90160-8, 1987.

879 Bonnet, S.: Dissolution of atmospheric iron in seawater, *Geophys. Res. Lett.*, 31(3), L03303,
880 doi:10.1029/2003GL018423, 2004.

881 ~~Boyd, P. W., Ibsanmi, E., Sander, S. G., Hunter, K. A. and Jackson, G. A.: Remineralization of upper ocean
882 particles: Implications for iron biogeochemistry, *Limnol. Oceanogr.*, 55(3), 1271–1288,
883 doi:10.4319/lom.2010.55.3.1271, 2010.~~

884 Boyle, E. A., Bergquist, B. A., Kayser, R. A. and Mahowald, N.: Iron, manganese, and lead at Hawaii Ocean
885 Time-series station ALOHA: Temporal variability and an intermediate water hydrothermal plume, *Geochim.
886 Cosmochim. Acta*, 69(4), 933–952, doi:10.1016/j.gca.2004.07.034, 2005.

887 Buck, C. S., Landing, W. M., Resing, J. A. and Measures, C. I.: The solubility and deposition of aerosol Fe and
888 other trace elements in the North Atlantic Ocean: Observations from the A16N CLIVAR/CO2repeat
889 hydrography section, *Mar. Chem.*, 120(1–4), 57–70, doi:10.1016/j.marchem.2008.08.003, 2010.

890 Cacador, I., Vale, C. and Catarino, F.: The influence of plants on concentration and fractionation of Zn, Pb, and
891 Cu in salt marsh sediments (Tagus Estuary, Portugal), *J. Aquat. Ecosyst. Heal.*, 5(3), 193–198,
892 doi:10.1007/BF00124106, 1996.

893 Collier, R. and Edmond, J.: The trace element geochemistry of marine biogenic particulate matter, *Prog.
894 Oceanogr.*, 13(2), 113–199, doi:10.1016/0079-6611(84)90008-9, 1984.

895 Cullen, J. T., Chong, M. and Ianson, D.: British columbia continental shelf as a source of dissolved iron to the
896 subarctic northeast Pacific Ocean, *Global Biogeochem. Cycles*, 23(4), 1–12, doi:10.1029/2008GB003326, 2009.

897 Cutter, G. A. and Bruland, K. W.: Rapid and noncontaminating sampling system for trace elements in global
898 ocean surveys, *Limnol. Oceanogr. Methods*, 10(JUNE), 425–436, doi:10.4319/lom.2012.10.425, 2012.

899 Dammshäuser, A., Wagener, T., Garbe-Schönberg, D. and Croot, P.: Particulate and dissolved aluminum and
900 titanium in the upper water column of the Atlantic Ocean, *Deep. Res. Part I Oceanogr. Res. Pap.*, 73, 127–139,
901 doi:10.1016/j.dsr.2012.12.002, 2013.

902 Dehairs, F., Jacquet, S., Savoye, N., Van Mooy, B. A. S., Buesseler, K. O., Bishop, J. K. B., Lamborg, C. H.,
903 Elskens, M., Baeyens, W., Boyd, P. W., Casciotti, K. L. and Monnin, C.: Barium in twilight zone suspended
904 matter as a potential proxy for particulate organic carbon remineralization: Results for the North Pacific, *Deep.
905 Res. Part II Top. Stud. Oceanogr.*, 55(14–15), 1673–1683, doi:10.1016/j.dsr2.2008.04.020, 2008.

906 Duarte, B., Silva, G., Costa, J. L., Medeiros, J. P., Azeda, C., Sá, E., Metelo, I., Costa, M. J. and Caçador, I.:
907 Heavy metal distribution and partitioning in the vicinity of the discharge areas of Lisbon drainage basins (Tagus
908 Estuary, Portugal), *J. Sea Res.*, 93(February), 101–111, doi:10.1016/j.seares.2014.01.003, 2014.

909 Dutay, J. C., Tagliabue, A., Kriest, I. and van Hulst, M. M. P.: Modelling the role of marine particle on large
910 scale 231Pa, 230Th, Iron and Aluminium distributions, *Prog. Oceanogr.*, 133, 66–72,
911 doi:10.1016/j.pocean.2015.01.010, 2015.

912 Dutkiewicz, A., Müller, R. D., O’Callaghan, S. and Jónasson, H.: Census of seafloor sediments in the world’s
913 ocean, *Geology*, 43(9), 795–798, doi:10.1130/G36883.1, 2015.

914 Eitrem, S., Thorndike, E. M. and Sullivan, L.: Turbidity distribution in the Atlantic Ocean, *Deep. Res.*
915 *Oceanogr. Abstr.*, 23(12), 1115–1127, doi:10.1016/0011-7471(76)90888-3, 1976.

916 Elderfield, H. and Schultz, A.: Mid-Ocean Ridge Hydrothermal Fluxes and the Chemical Composition of the
917 Ocean, *Annu. Rev. Earth Planet. Sci.*, 24(1), 191–224, doi:10.1146/annurev.earth.24.1.191, 1996.

918 Ellwood, M. J., Nodder, S. D., King, A. L., Hutchins, D. A., Wilhelm, S. W. and Boyd, P. W.: Pelagic iron
919 cycling during the subtropical spring bloom, east of New Zealand, *Mar. Chem.*, 160, 18–33,
920 doi:10.1016/j.marchem.2014.01.004, 2014.

921 Elrod, V. A., Berelson, W. M., Coale, K. H. and Johnson, K. S.: The flux of iron from continental shelf
922 sediments: A missing source for global budgets, *Geophys. Res. Lett.*, 31(12), 2–5, doi:10.1029/2004GL020216,
923 2004.

924 [Fitzsimmons, J. N., John, S. G., Marsay, C. M., Hoffman, C. L., Nicholas, S. L., Toner, B. M., German, C. R.
925 and Sherrell, R. M.: Iron persistence in a distal hydrothermal plume supported by dissolved-particulate
926 exchange, *Nat. Geosci.*, 10\(3\), 195–201, doi:10.1038/ngeo2900, 2017.](#)

927 Fitzwater, S. E., Johnson, K. S., Gordon, R. M., Coale, K. H. and Smith, W. O.: Trace metal concentrations in
928 the Ross Sea and their relationship with nutrients and phytoplankton growth, *Deep. Res. Part II Top. Stud.*
929 *Oceanogr.*, 47(15–16), 3159–3179, doi:10.1016/S0967-0645(00)00063-1, 2000.

930 Frago, G. M., Poulton, A. J., Yashayaev, I. M., Head, E. J. H., Stinchcombe, M. C. and Purdie, D. A.:
931 Biogeographical patterns and environmental controls of phytoplankton communities from contrasting
932 hydrographical zones of the Labrador Sea, *Prog. Oceanogr.*, 141, 212–226, doi:10.1016/j.pocean.2015.12.007,
933 2016.

934 Frew, R. D., Hutchins, D. A., Nodder, S., Sanudo-Wilhelmy, S., Tovar-Sanchez, A., Leblanc, K., Hare, C. E.
935 and Boyd, P. W.: Particulate iron dynamics during FeCycle in subantarctic waters southeast of New Zealand,
936 *Global Biogeochem. Cycles*, 20(1), 1–15, doi:10.1029/2005GB002558, 2006.

937 [Fung, I. Y., Meyn, S. K., Tegen, I., Doney, S. C., John, J. G., & Bishop, J. K.: Iron supply and demand in the
938 upper ocean, *Global Biogeochem. Cycles*, 14\(1\), 281–295, doi:10.1029/1999GB900059, 2000.](#)

- 939 García-Ibáñez, M. I., Pardo, P. C., Carracedo, L. I., Mercier, H., Lherminier, P., Ríos, A. F. and Pérez, F. F.:
940 Structure, transports and transformations of the water masses in the Atlantic Subpolar Gyre, *Prog. Oceanogr.*,
941 135, 18–36, doi:10.1016/j.pocean.2015.03.009, 2015.
- 942 Gardner, W. D., Tucholke, B. E., Richardson, M. J. and Biscaye, P. E.: Benthic storms, nepheloid layers, and
943 linkage with upper ocean dynamics in the western North Atlantic, *Mar. Geol.*, 385, 304–327,
944 doi:10.1016/j.margeo.2016.12.012, 2017.
- 945 Gardner, W. D., Richardson, M. J. and Mishonov, A. V.: Global assessment of benthic nepheloid layers and
946 linkage with upper ocean dynamics, *Earth Planet. Sci. Lett.*, 482, 126–134, doi:10.1016/j.epsl.2017.11.008,
947 2018.
- 948 Gerringa, L. J. A., Rijkenberg, M. J. A., Schoemann, V., Laan, P. and de Baar, H. J. W.: Organic complexation
949 of iron in the West Atlantic Ocean, *Mar. Chem.*, 177, 434–446, doi:10.1016/j.marchem.2015.04.007, 2015.
- 950 ~~Guieu, C., Martin, J. M., Thomas, A. J. and Elbaz Poulichet, F.: Atmospheric versus river inputs of metals to the~~
951 ~~Gulf of Lions. Total concentrations, partitioning and fluxes. *Mar. Pollut. Bull.*, 22(4), 176–183,~~
952 ~~doi:10.1016/0025-326X(91)90467-7, 1991.~~
- 953 Hawkings, J. R., Wadham, J. L., Tranter, M., Raiswell, R., Benning, L. G., Statham, P. J., Tedstone, A.,
954 Nienow, P., Lee, K. and Telling, J.: Ice sheets as a significant source of highly reactive nanoparticulate iron to
955 the oceans, *Nat. Commun.*, 5(May), 1–8, doi:10.1038/ncomms4929, 2014.
- 956 Hwang, J., Druffel, E. R. M. and Eglinton, T. I.: Widespread influence of resuspended sediments on oceanic
957 particulate organic carbon: Insights from radiocarbon and aluminum contents in sinking particles, *Global*
958 *Biogeochem. Cycles*, 24(4), 1–10, doi:10.1029/2010GB003802, 2010.
- 959 Jeandel, C. and Oelkers, E. H.: The influence of terrigenous particulate material dissolution on ocean chemistry
960 and global element cycles, *Chem. Geol.*, 395, 50–66, doi:10.1016/j.chemgeo.2014.12.001, 2015.
- 961 Jeandel, C., Peucker-Ehrenbrink, B., Jones, M. T., Pearce, C. R., Oelkers, E. H., Godderis, Y., Lacan, F.,
962 Aumont, O. and Arsouze, T.: Ocean margins: The missing term in oceanic element budgets?, *Eos, Transactions*
963 *American Geophysical Union*, 92(26), 217–224, doi: 10.1029/2011EO260001, 2011.
- 964 Jickells, T. D., An, Z. S., Andersen, K. K., Baker, A. R., Bergametti, C., Brooks, N., Cao, J. J., Boyd, P. W.,
965 Duce, R. A., Hunter, K. A., Kawahata, H., Kubilay, N., LaRoche, J., Liss, P. S., Mahowald, N., Prospero, J. M.,
966 Ridgwell, A. J., Tegen, I. and Torres, R.: Global iron connections between desert dust, ocean biogeochemistry,
967 and climate, *Science* (80-.), 308(5718), 67–71, doi:10.1126/science.1105959, 2005.
- 968 Jouanneau, J. M., Garcia, C., Oliveira, A., Rodrigues, A., Dias, J. A. and Weber, O.: Dispersal and deposition of
969 suspended sediment on the shelf off the Tagus and Sado estuaries, S.W. Portugal, *Prog. Oceanogr.*, 42(1–4),
970 233–257, doi:10.1016/S0079-6611(98)00036-6, 1998.

971 Labatut, M., Lacan, F., Pradoux, C., Chmeleff, J., Radic, A., Murray, J. W., Poitrasson, F., Johansen, A. M.,
972 Thil, F., Lacan, F., Pradoux, C., Chmeleff, J., Radic, A., Murray, J. W., Poitrasson, F., Johansen, A. M. and
973 Thil, F.: Iron sources and dissolved - particulate interactions in the seawater of the Western Equatorial Pacific,
974 iron isotope perspectives., *Global Biogeochemical Cycles*, 1044–1065, doi:10.1002/2014GB004928, 2014.

975 Lam, P. J. and Bishop, J. K. B.: The continental margin is a key source of iron to the HNLC North Pacific
976 Ocean, *Geophys. Res. Lett.*, 35(7), 1–5, doi:10.1029/2008GL033294, 2008.

977 Lam, P. J., Ohnemus, D. C. and Marcus, M. A.: The speciation of marine particulate iron adjacent to active and
978 passive continental margins, *Geochim. Cosmochim. Acta*, 80, 108–124, doi:10.1016/j.gca.2011.11.044, 2012.

979 Lam, P. J., Ohnemus, D. C. and Auro, M. E.: Size-fractionated major particle composition and concentrations
980 from the US GEOTRACES North Atlantic Zonal Transect, *Deep. Res. Part II Top. Stud. Oceanogr.*, 116, 303–
981 320, doi:10.1016/j.dsr2.2014.11.020, 2015.

982 Lam, P. J., Lee, J. M., Heller, M. I., Mehic, S., Xiang, Y. and Bates, N. R.: Size-fractionated distributions of
983 suspended particle concentration and major phase composition from the U.S. GEOTRACES Eastern Pacific
984 Zonal Transect (GP16), *Mar. Chem.*, (April), 0–1, doi:10.1016/j.marchem.2017.08.013, 2017.

985 Lannuzel, D., Bowie, A. R., van der Merwe, P. C., Townsend, A. T. and Schoemann, V.: Distribution of
986 dissolved and particulate metals in Antarctic sea ice, *Mar. Chem.*, 124(1–4), 134–146,
987 doi:10.1016/j.marchem.2011.01.004, 2011.

988 Lannuzel, D., Van der Merwe, P. C., Townsend, A. T. and Bowie, A. R.: Size fractionation of iron, manganese
989 and aluminium in Antarctic fast ice reveals a lithogenic origin and low iron solubility, *Mar. Chem.*, 161, 47–56,
990 doi:10.1016/j.marchem.2014.02.006, 2014.

991 Lee, J. M., Heller, M. I. and Lam, P. J.: Size distribution of particulate trace elements in the U.S. GEOTRACES
992 Eastern Pacific Zonal Transect (GP16), *Mar. Chem.*, 201(September 2017), 108–123,
993 doi:10.1016/j.marchem.2017.09.006, 2017.

994 Lemaître, N., planquette, H., Planchon, F., Sarthou, G., Jacquet, S., Garcia-Ibanez, M. I., Gourain, A., Cheize,
995 M., Monin, L., Andre, L., Laha, P., Terryn, H., and Dehairs, F.: Particulate barium tracing significant
996 mesopelagic carbon remineralisation in the North Atlantic, *Biogeosciences Discussions*, doi:10.5194/bg-15-
997 2289-2018, 2018a.

998 Lemaitre, N., Planchon, F., Planquette, H., Dehairs, F., Fonseca-Batista, D., Roukaerts, A., Deman, F., Tang, Y.,
999 Mariez, C., and Sarthou G.: High variability of export fluxes along the North Atlantic GEOTRACES section
1000 GA01: Particulate organic carbon export deduced from the 234Th method, *Biogeosciences Discuss.*,
1001 doi:10.5194/bg-2018-190, 2018b.

1002 Le Roy, E., Sanial, V., Charette, M.A., Van Beek, P., Lacan, F., Jacquet, S.H., Henderson, P.B., Souhaut, M.,
1003 García-Ibáñez, M.I., Jeandel, C. and Pérez, F.: The 226Ra-Ba relationship in the North Atlantic during
1004 GEOTRACES-GA01, Biogeosciences Discussions, doi:10.5194/bg-2017-478, 2017.

1005 Loring, D. H. and Asmund, G.: Geochemical factors controlling accumulation of major and trace elements in
1006 Greenland coastal and fjord sediments, Environ. Geol., 28(1), 2–11, doi:10.1007/s002540050072, 1996.

1007 Mahowald, N. M., Baker, A. R., Bergametti, G., Brooks, N., Duce, R. A., Jickells, T. D., Kubilay, N., Prospero,
1008 J. M. and Tegen, I.: Atmospheric global dust cycle and iron inputs to the ocean, Global Biogeochem. Cycles,
1009 19(4), doi:10.1029/2004GB002402, 2005.

1010 Marsay, C. M., Lam, P. J., Heller, M. I., Lee, J. M. and John, S. G.: Distribution and isotopic signature of
1011 ligand-leachable particulate iron along the GEOTRACES GP16 East Pacific Zonal Transect, Mar. Chem.,
1012 (November 2016), 1–14, doi:10.1016/j.marchem.2017.07.003, 2017.

1013 ~~Martin, J. and Meybeck, M.: Elemental mass balance of material carried by major world rivers, Marine
1014 chemistry, 7, 173–206, 1979.~~

1015 Martin, J. H., Fitzwater, S. E., Michael Gordon, R., Hunter, C. N. and Tanner, S. J.: Iron, primary production
1016 and carbon-nitrogen flux studies during the JGOFS North Atlantic bloom experiment, Deep. Res. Part II, 40(1–
1017 2), 115–134, doi:10.1016/0967-0645(93)90009-C, 1993.

1018 McCave, I. N. and Hall, I. R.: Turbidity of waters over the Northwest Iberian continental margin, Prog.
1019 Oceanogr., 52(2–4), 299–313, doi:10.1016/S0079-6611(02)00012-5, 2002.

1020 Menzel Barraqueta, J.L., Schlosser, C., Planquette, H., Gourain, A., Cheize, M., Boutorh, J., Shelley, R., Pereira
1021 Contreira, L., Gledhill, M., Hopwood, M.J. and Lherminier, P.: Aluminium in the North Atlantic Ocean and the
1022 Labrador Sea (GEOTRACES GA01 section): roles of continental inputs and biogenic particle removal.
1023 Biogeosciences Discussions, 1-28, doi: 10.5194/bg-2018-39, 2018.

1024 Milne, A., Schlosser, C., Wake, B. D., Achterberg, E. P., Chance, R., Baker, A. R., Forryan, A. and Lohan, M.
1025 C.: Particulate phases are key in controlling dissolved iron concentrations in the (sub)tropical North Atlantic,
1026 Geophys. Res. Lett., 44(5), 2377–2387, doi:10.1002/2016GL072314, 2017.

1027 Mudie, P. J., Keen, C. E., Hardy, I. A. and Vilks, G.: Multivariate analysis and quantitative paleoecology of
1028 benthic foraminifera in surface and Late Quaternary shelf sediments, northern Canada, Mar. Micropaleontol.,
1029 8(4), 283–313, doi:10.1016/0377-8398(84)90018-5, 1984.

1030 Nuester, J., Shema, S., Vermont, A., Fields, D. M. and Twining, B. S.: The regeneration of highly bioavailable
1031 iron by meso- and microzooplankton, , 59(4), 1399–1409, doi:10.4319/lo.2014.59.4.1399, 2014.

1032 Oelkers, E. H., Jones, M. T., Pearce, C. R., Jeandel, C., Eiriksdottir, E. S. and Gislason, S. R.: Riverine
1033 particulate material dissolution in seawater and its implications for the global cycles of the elements, Geosci.,
1034 344(11–12), 646–651, doi:10.1016/j.crte.2012.08.005, 2012.

- 1035 Ohnemus, D. C. and Lam, P. J.: Cycling of lithogenic marine particles in the US GEOTRACES North Atlantic
1036 transect, *Deep. Res. Part II Top. Stud. Oceanogr.*, 116, 283–302, doi:10.1016/j.dsr2.2014.11.019, 2015.
- 1037 Peers, G. and Price, N. M.: A role for manganese in superoxide dismutases and growth of iron-deficient
1038 diatoms, *Limnol. Oceanogr.*, 49(5), 1774–1783, doi:10.4319/lo.2004.49.5.1774, 2004.
- 1039 Planquette, H. and Sherrell, R. M.: Sampling for particulate trace element determination using water sampling
1040 bottles: Methodology and comparison to in situ pumps, *Limnol. Oceanogr. Methods*, 10(5), 367–388,
1041 doi:10.4319/lom.2012.10.367, 2012.
- 1042 Planquette, H., Fones, G. R., Statham, P. J. and Morris, P. J.: Origin of iron and aluminium in large particles (>
1043 53 μm) in the Crozet region, Southern Ocean, *Mar. Chem.*, 115(1–2), 31–42,
1044 doi:10.1016/j.marchem.2009.06.002, 2009.
- 1045 Planquette, H., Sanders, R. R., Statham, P. J., Morris, P. J. and Fones, G. R.: Fluxes of particulate iron from the
1046 upper ocean around the Crozet Islands: A naturally iron-fertilized environment in the Southern Ocean, *Global
1047 Biogeochem. Cycles*, 25(2), doi:10.1029/2010GB003789, 2011.
- 1048 Planquette, H., Sherrell, R. M., Stammerjohn, S. and Field, M. P.: Particulate iron delivery to the water column
1049 of the Amundsen Sea, Antarctica, *Mar. Chem.*, 153, 15–30, doi:10.1016/j.marchem.2013.04.006, 2013.
- 1050 Radic, A., Lacan, F. and Murray, J. W.: Iron isotopes in the seawater of the equatorial Pacific Ocean: New
1051 constraints for the oceanic iron cycle, *Earth Planet. Sci. Lett.*, 306(1–2), 1–10, doi:10.1016/j.epsl.2011.03.015,
1052 2011.
- 1053 Raiswell, R., Benning, L. G., Tranter, M. and Tulaczyk, S.: Bioavailable iron in the Southern Ocean: The
1054 significance of the iceberg conveyor belt, *Geochem. Trans.*, 9(1), 7, doi:10.1186/1467-4866-9-7, 2008.
- 1055 ~~Resing, J. A., Sedwick, P. N., German, C. R., Jenkins, W. J., Moffett, J. W., Sohst, B. M. and Tagliabue, A.:
1056 Basin-scale transport of hydrothermal dissolved metals across the South Pacific Ocean, *Nature*, 523(7559), 200–
1057 203, doi:10.1038/nature14577, 2015.~~
- 1058 ~~Revels, B. N., Ohnemus, D. C., Lam, P. J., Conway, T. M. and John, S. G.: The isotopic signature and
1059 distribution of particulate iron in the North Atlantic Ocean, *Deep. Res. Part II Top. Stud. Oceanogr.*, 116, 321–
1060 331, doi:10.1016/j.dsr2.2014.12.004, 2015.~~
- 1061 Rijkenberg, M. J. A., Middag, R., Laan, P., Gerringa, L. J. A., Van Aken, H. M., Schoemann, V., De Jong, J. T.
1062 M. and De Baar, H. J. W.: The distribution of dissolved iron in the West Atlantic Ocean, *PLoS One*, 9(6), 1–14,
1063 doi:10.1371/journal.pone.0101323, 2014.
- 1064 Rutgers Van Der Loeff, M. M., Meyer, R., Rudels, B. and Rachor, E.: Resuspension and particle transport in the
1065 benthic nepheloid layer in and near Fram Strait in relation to faunal abundances and ^{234}Th depletion, *Deep.
1066 Res. Part I Oceanogr. Res. Pap.*, 49(11), 1941–1958, doi:10.1016/S0967-0637(02)00113-9, 2002.

1067 Sanders, R., Henson, S. A., Koski, M., De La Rocha, C. L., Painter, S. C., Poulton, A. J., Riley, J., Salihoglu, B.,
1068 Visser, A., Yool, A., Bellerby, R. and Martin, A. P.: The Biological Carbon Pump in the North Atlantic, *Prog.*
1069 *Oceanogr.*, 129(PB), 200–218, doi:10.1016/j.pocean.2014.05.005, 2014.

1070 Sarthou, G., Vincent, D., Christaki, U., Obernosterer, I., Timmermans, K. R. and Brussaard, C. P. D.: The fate
1071 of biogenic iron during a phytoplankton bloom induced by natural fertilisation: Impact of copepod grazing,
1072 *Deep. Res. Part II Top. Stud. Oceanogr.*, 55(5–7), 734–751, doi:10.1016/j.dsr2.2007.12.033, 2008.

1073 Schlosser, C., Schmidt, K., Aquilina, A., Homoky, W. B., Castrillejo, M., Mills, R. A., Patey, M. D., Fielding,
1074 S., Atkinson, A. and Achterberg, E. P.: Mechanisms of dissolved and labile particulate iron supply to shelf
1075 waters and phytoplankton blooms off South Georgia, Southern Ocean, *Biogeosciences Discuss.*, 0049(July), 1–
1076 49, doi:10.5194/bg-2017-299, 2017.

1077 Shelley, R. U., Landing, W. M., Ussher, S. J., Planquett, H. and Sarthou, G.: Characterisation of aerosol
1078 provenance from the fractional solubility of Fe (Al, Ti, Mn, Co, Ni, Cu, Zn, Cd and Pb) in North Atlantic
1079 aerosols (GEOTRACES GA01 and GA03), *Biogeosciences*, submitted(November), 1–31, doi:10.5194/bg-
1080 2017-415, 2017.

1081 Shelley, R. U., Landing, W. M., Ussher, S. J., Planquette, H. and Sarthou, G.: Regional trends in the fractional
1082 solubility of Fe and other metals from North Atlantic aerosols (GEOTRACES cruises GA01 and GA03)
1083 following a two-stage leach, *Biogeosciences*, 155194(1), 2271–2288, doi:10.5194/bg-15-2271-2018, 2018.

1084 Sherrell, R. M., Field, P. M. and Gao, Y.: Temporal variability of suspended mass and composition in the
1085 Northeast Pacific water column: Relationships to sinking flux and lateral advection, *Deep. Res. Part II Top.*
1086 *Stud. Oceanogr.*, 45(4–5), 733–761, doi:10.1016/S0967-0645(97)00100-8, 1998.

1087 Spinrad, R. W., Zaneveld, J. R. and Kitchen, J.C.: A Study of the Optical Characteristics of the Suspended
1088 Particles Benthic N epheloid Layer of the Scotian Rise, *J. Geophys. Res.*, 88, 7641–7645, doi:0148-
1089 0227/83/003C, 1983.

1090 Statham, P. J., Skidmore, M. and Tranter, M.: Inputs of glacially derived dissolved and colloidal iron to the
1091 coastal ocean and implications for primary productivity, *Global Biogeochem. Cycles*, 22(3), 1–11,
1092 doi:10.1029/2007GB003106, 2008.

1093 Straneo, F., Pickart, R. S. and Lavender, K.: Spreading of Labrador sea water: An advective-diffusive study
1094 based on Lagrangian data, *Deep. Res. Part I Oceanogr. Res. Pap.*, 50(6), 701–719, doi:10.1016/S0967-
1095 0637(03)00057-8, 2003.

1096 [Strzepek, R. F., Maldonado, M. T., Higgins, J. L., Hall, J., Safi, K., Wilhelm, S. W. and Boyd, P. W.: Spinning](#)
1097 [the “ferrous wheel”: The importance of the microbial community in an iron budget during the FeCycle](#)
1098 [experiment, *Global Biogeochem. Cycles*, 19\(4\), doi:10.1029/2005GB002490, 2005.](#)

1099 Sunda, W. G. and Huntsman, S. A.: Effect of Competitive Interactions Between Manganese and Copper on
1100 Cellular Manganese and Growth in Estuarine and Oceanic Species of the Diatom *Thalassiosira*, *Limnol.*
1101 *Oceanogr.*, 28(5), 924–934, doi:10.4319/lo.1983.28.5.0924, 1983.

1102 Tagliabue, A., Bopp, L., Dutay, J. C., Bowie, A. R., Chever, F., Jean-Baptiste, P., Bucciarelli, E., Lannuzel, D.,
1103 Remenyi, T., Sarthou, G., Aumont, O., Gehlen, M. and Jeandel, C.: Hydrothermal contribution to the oceanic
1104 dissolved iron inventory, *Nat. Geosci.*, 3(4), 252–256, doi:10.1038/ngeo818, 2010.

1105 ~~Tagliabue, A., Williams, R. G., Rogan, N., Achterberg, E. P. and Boyd, P. W.: A ventilation-based frame work~~
1106 ~~to explain the regeneration-scavenging balance of iron in the ocean., 7227–7236, doi:10.1002/2014GL061066.~~
1107 ~~2014.~~

1108 Tagliabue, A., Bowie, A. R., Boyd, P. W., Buck, K. N., Johnson, K. S. and Saito, M. A.: The integral role of
1109 iron in ocean biogeochemistry, *Nature*, 543(7643), 51–59, doi:10.1038/nature21058, 2017.

1110 Taylor, S. . and McLennan, S. .: The geochemical evolution of the continental crust, *Rev. Geophys.*, 33(2), 241–
1111 265, doi:10.1029/95RG00262, 1995.

1112 Tebo, B. M. and Emerson, S. R.: Effect of Oxygen Tension Manganese (II) Concentration and Temperature on
1113 the Microbially Catalyzed Manganese-Ii Oxidation Rate in a Marine Fjord, *Appl. Environ. Microbiol.*, 50(5),
1114 1268–1273, 1985.

1115 Tebo, B. M., Nealson, K. H., Emerson, S. and Jacobs, L.: Microbial mediation of Mn(II) and Co(II)
1116 precipitation at the o₂/H₂S interfaces in two anoxic fjords, 29(6), 1247–1258, 1984.

1117 Tonnard, M., Planquette, H., Bowie, A. R., van der Merwe, P., Gallinari, M., Desprez de Gésincourt, F.,
1118 Germain, Y., Gourain, A., Benetti, M., Reverdin, G., Tréguer, P., Boutorh, J., Cheize, M., Menzel Barraqueta,
1119 J., Pereira-Contreira, L., Shelley, R., Lherminier, P., and Sarthou, G.: Dissolved iron in the North Atlantic
1120 Ocean and Labrador Sea along the GEOVIDE section (GEOTRACES section GA01), *Biogeosciences Discuss.*,
1121 <https://doi.org/10.5194/bg-2018-147>, 2018

1122 Trefry, J. H., Trocine, R. P., Klinkhammer, G. P. and Rona, P. A.: Iron and copper enrichment of suspended
1123 particles in dispersed hydrothermal plumes along the mid-Atlantic Ridge, *Geophys. Res. Lett.*, 12(8), 506–
1124 509, doi:10.1029/GL012i008p00506, 1985.

1125 Ussher, S. J., Achterberg, E. P. and Worsfold, P. J.: Marine biogeochemistry of iron, *Environ. Chem.*, 1(2), 67–
1126 80, doi:10.1071/EN04053, 2004.

1127 Ussher, S. J., Worsfold, P. J., Achterberg, E. P., Laës, A., Blain, S., Laan, P., de Baar, H. J. W., ~~Lae, A., Laan,~~
1128 ~~P., Baar, H. J. W. De, Laës, A., Blain, S., Laan, P., de Baar, H. J. W., Lac, A., Laan, P. and Baar, H. J. W. De:~~
1129 Distribution and redox speciation of dissolved iron on the European continental margin, *Limnol. Oceanogr.*,
1130 52(6), 2530–2539, doi:10.4319/lo.2007.52.6.2530, 2007.

1131 Van der Merwe, P., Lannuzel, D., Bowie, A. R., Mancuso Nichols, C. A. and Meiners, K. M.: Iron fractionation
1132 in pack and fast ice in East Antarctica: Temporal decoupling between the release of dissolved and particulate
1133 iron during spring melt, *Deep. Res. Part II Top. Stud. Oceanogr.*, 58(9–10), 1222–1236,
1134 doi:10.1016/j.dsr2.2010.10.036, 2011a.

1135 Van Der Merwe, P., Lannuzel, D., Bowie, A. R. and Meiners, K. M.: High temporal resolution observations of
1136 spring fast ice melt and seawater iron enrichment in East Antarctica, *J. Geophys. Res. Biogeosciences*, 116(3),
1137 1–18, doi:10.1029/2010JG001628, 2011b.

1138 Weinstein, S. E. and Moran, S. B.: Distribution of size-fractionated particulate trace metals collected by bottles
1139 and in-situ pumps in the Gulf of Maine-Scotian Shelf and Labrador Sea, *Mar. Chem.*, 87(3–4), 121–135,
1140 doi:10.1016/j.marchem.2004.02.004, 2004.

1141 Yashayaev, I.: Hydrographic changes in the Labrador Sea, 1960–2005, *Prog. Oceanogr.*, 73(3–4), 242–276,
1142 doi:10.1016/j.pocean.2007.04.015, 2007.

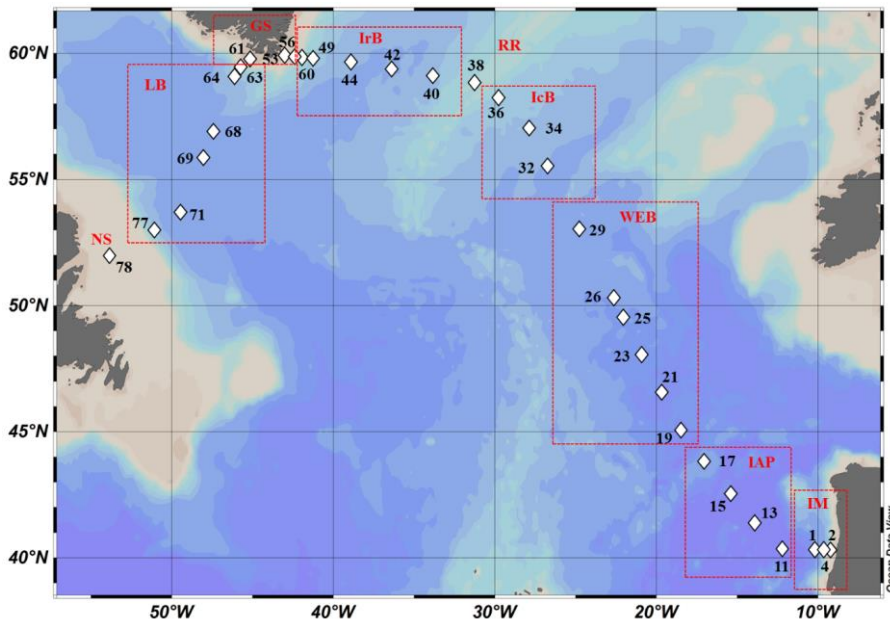
1143 Yashayaev, I. and Loder, J. W.: Enhanced production of Labrador Sea Water in 2008, *Geophys. Res. Lett.*,
1144 36(1), doi:10.1029/2008GL036162, 2009.

1145 Zunino, P., Lherminier, P., Mercier, H., Daniault, N., García-Ibáñez, M. I., and Pérez, F. F.: The GEOVIDE
1146 cruise in May–June 2014 reveals an intense Meridional Overturning Circulation over a cold and fresh subpolar
1147 North Atlantic. *Biogeosciences*, 14(23), 5323, 2017.

1148
1149
1150
1151
1152
1153
1154
1155
1156
1157
1158
1159
1160
1161
1162
1163
1164
1165
1166
1167

1168
1169
1170
1171
1172
1173
1174
1175
1176
1177
1178
1179
1180
1181
1182

1183 Figure 1: Map of stations where suspended particle samples were collected with GO-FLO bottles during the
1184 GEOVIDE cruise (GA01). Biogeochemical provinces are indicated by red squares, IM: Iberian Margin, IAP: Iberian
1185 Abyssal Plain, WEB: Western European Basin, IcB: Iceland Basin, RR: Reykjanes Ridge, IrB: Irminger Basin, GS:
1186 Greenland Shelf, LB: Labrador Basin, NS: Newfoundland Shelf. This figure was generated by Ocean Data View
1187 (Schlitzer, R., Ocean Data View, odv.awi.de, 2017).

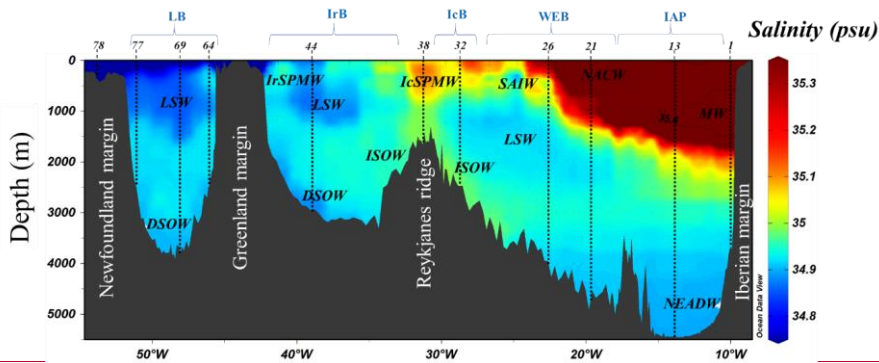


1188
1189
1190
1191

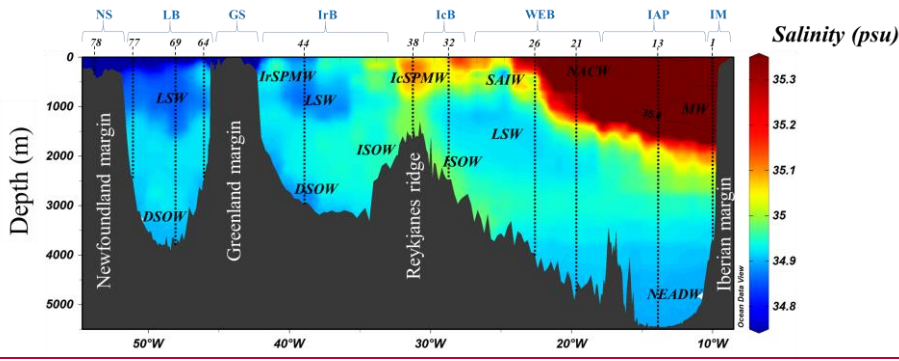
1192
 1193
 1194
 1195
 1196
 1197
 1198
 1199
 1200
 1201
 1202
 1203

1204 **Figure 2: Salinity section during the GEOVIDE cruise. Water masses are indicated in black, MW: Mediterranean**
 1205 **Water; NACW: North Atlantic Central Water; NEADW: North East Atlantic Deep Water; LSW: Labrador Sea**
 1206 **Water; ISOW: Iceland-Scotland Overflow Water; SAIW: Sub-Arctic Intermediate Water; IcSPMW: Iceland Sub-**
 1207 **Polar Mode Water; IrSPMW: Irminger Sub-Polar Mode Water. Stations locations are indicated by the numbers.**
 1208 **Biogeochemical provinces are indicated in blue font above station numbers. Contour of salinity = 35.8psu have been**
 1209 **apply to identify the Mediterranean Water. This figure was generated by Ocean Data View (Schlitzer, R., Ocean Data**
 1210 **View, odv.awi.de, 2017).**

1211

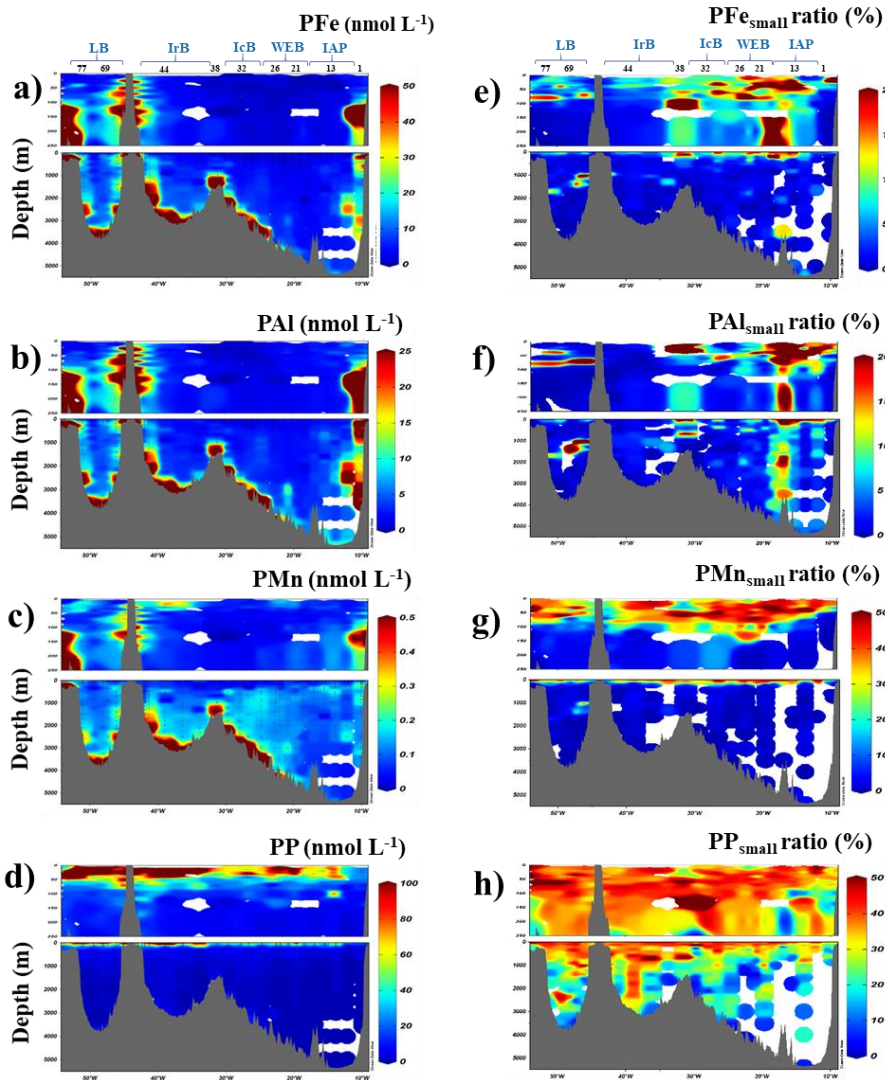


1212



1213
1214
1215
1216
1217
1218
1219
1220
1221
1222
1223
1224
1225
1226
1227
1228
1229
1230
1231
1232

1233 Figure 3: Left) Distribution of total particulate iron (a, PFe), aluminium (b, PAI), manganese (c, PMn) and
 1234 phosphorus (d, PP) concentrations (in nmol L^{-1}) along the GEOVIDE section. Right) Contribution of small size
 1235 fraction (0,45-5 μm) expressed as percentage (%) of the total concentration of PFe (e), PAI (f), PMn (g) and PP (h).
 1236 Station IDs and biogeochemical region are indicated on top of section a. This figure was generated by Ocean Data
 1237 View (Schlitzer, R., Ocean Data View, odv.awi.de, 2017).



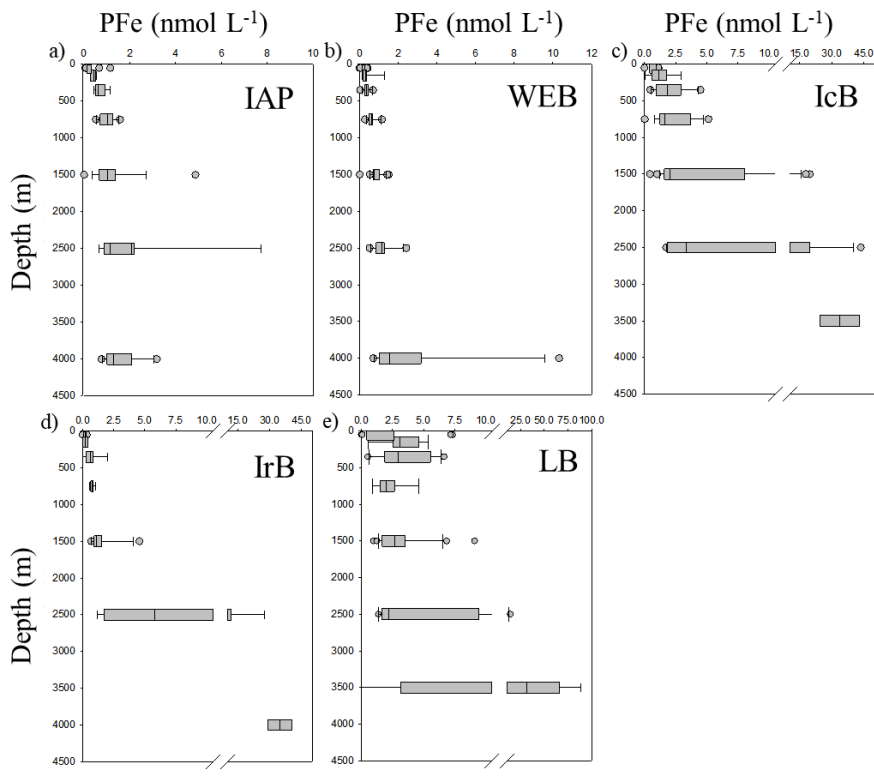
1238

1239

1240

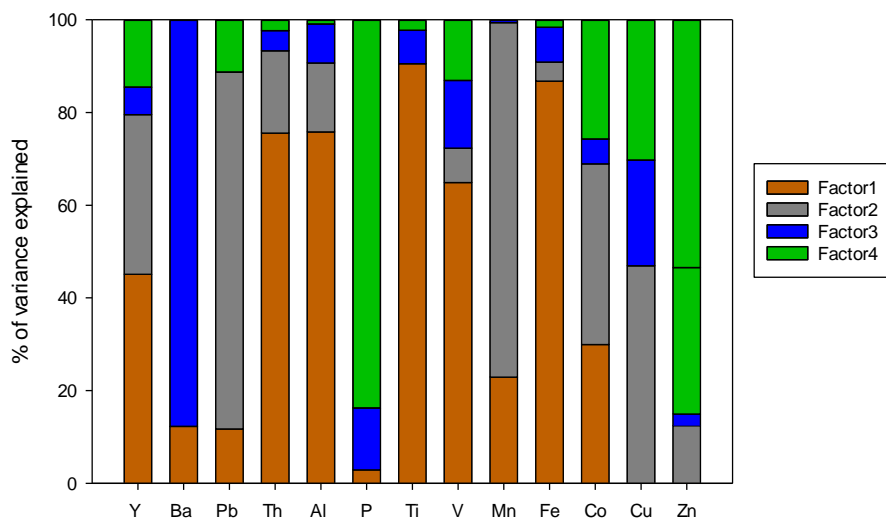
1241

1242 Figure 4: Boxplot figure of the particulate iron vertical profile (in nmol L^{-1}) in the a) Iberian abyssal plain (IAP), b)
 1243 Western European basin (WEB), c) Icelandic basin (IcB), d) Irminger basin (IrB) and e) Labrador basins (LB). The
 1244 left boundary of the box represents the 25th percentile while the right boundary represents the 75th percentile, the line
 1245 within the box marks the median value. Whiskers represent the 90th and 10th percentiles and dots are the outlying
 1246 data. Seven depth boxes have been used (0-100m, 100-200m, 200-500m, 500-1000m, 1000-2000m, 2000-3000m and
 1247 3000m-bottom depth).



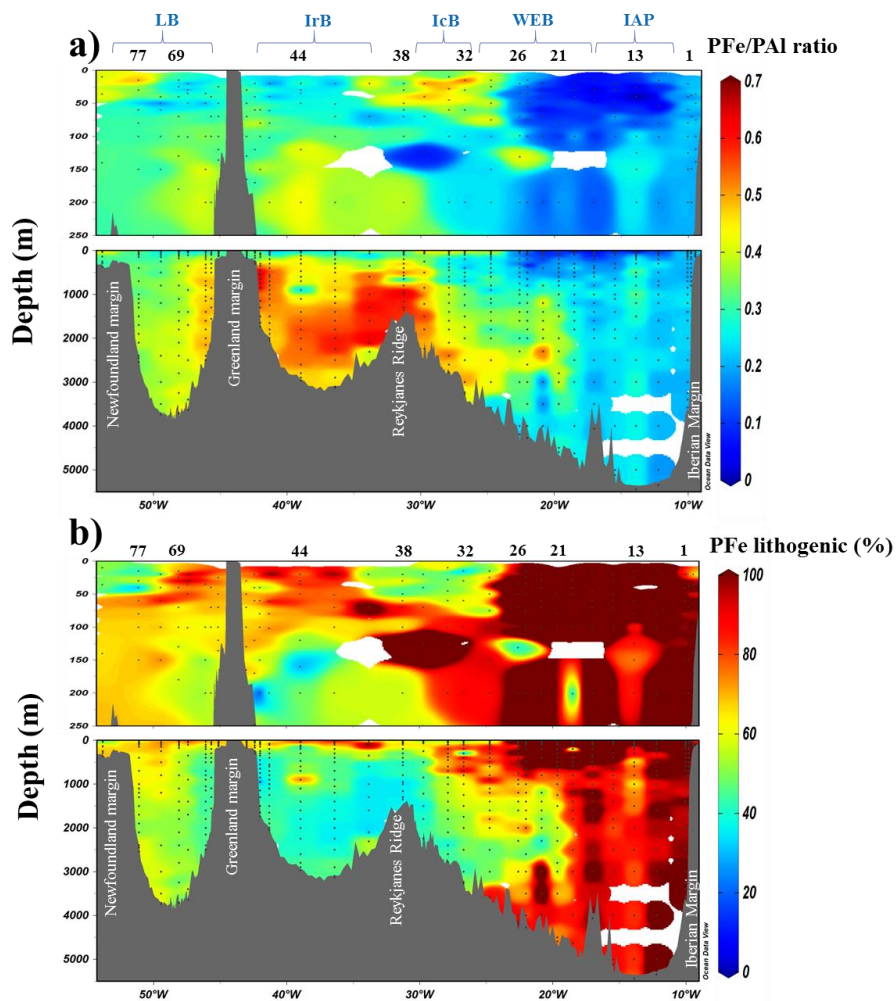
1248
 1249
 1250
 1251
 1252
 1253
 1254
 1255
 1256
 1257
 1258
 1259
 1260

1261 Figure 5: Factor fingerprint of the positive matrix factorisation. The four factors are represented in a stacked bar
1262 chart of the percentage of variance explained per element.



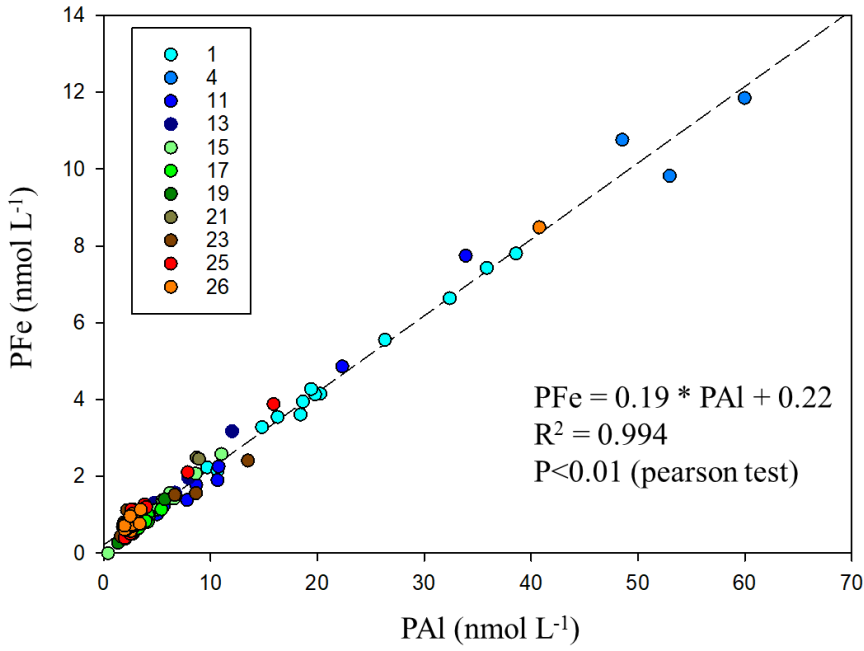
1263
1264
1265
1266
1267
1268
1269
1270
1271
1272
1273
1274
1275
1276
1277
1278
1279
1280
1281

1282 Figure 6: a) Section of the PFe to PAI molar ratio (mol mol^{-1}); (b) contribution of lithogenic PFe (%) based on Eq. (1).
 1283 Station IDs and biogeochemical provinces are indicated above each section. This figure was generated by Ocean Data
 1284 View (Schlitzer, R., Ocean Data View, odv.awi.de, 2017).



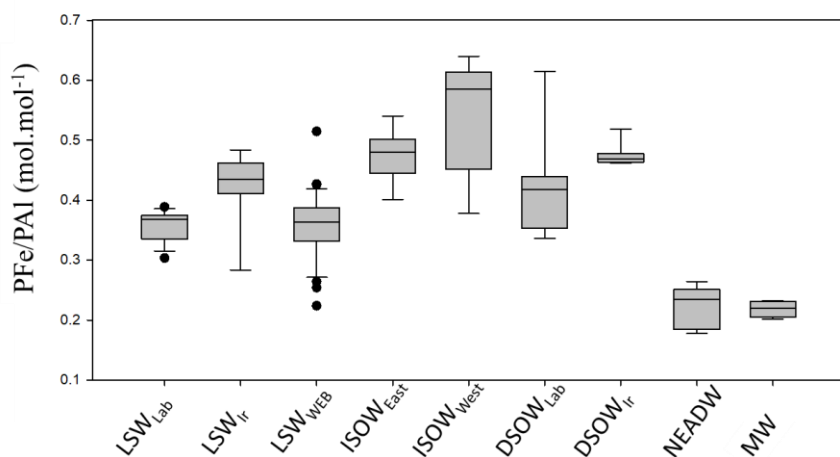
1285
 1286
 1287
 1288
 1289
 1290
 1291

1292 **Figure 7: PFe over PAI concentrations (nmol L⁻¹) for all stations located in the Iberian Abyssal Plain and Western**
1293 **European Basin. Note that the total concentrations of the two elements covaried strongly.**



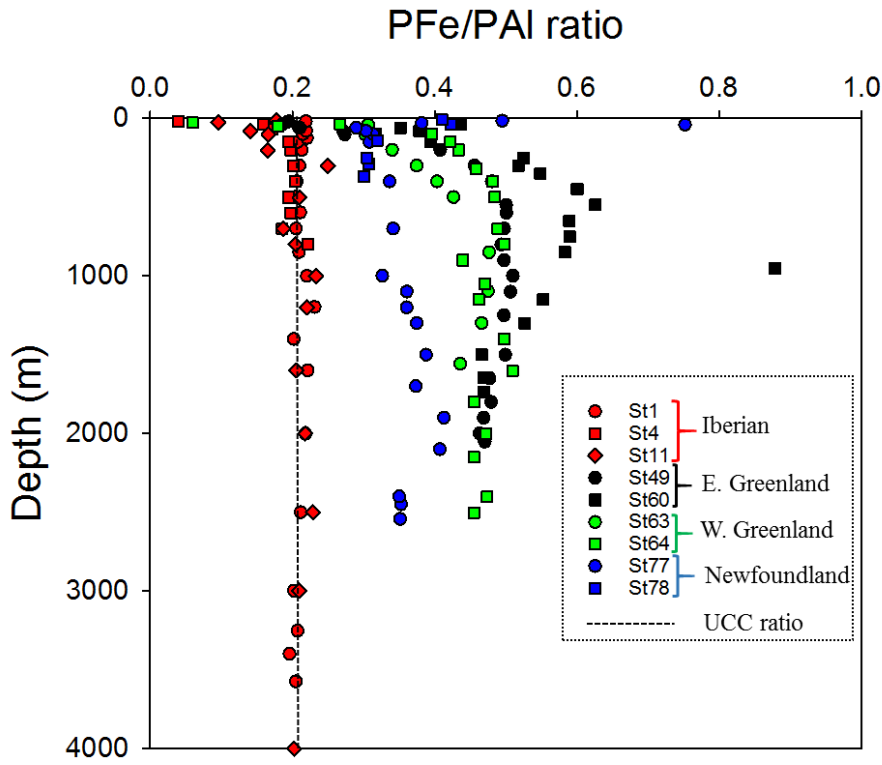
1294
1295
1296
1297
1298
1299
1300
1301
1302
1303
1304
1305
1306

1307 Figure 87: Whisker diagram of PFe/PAI molar ratio (mol mol^{-1}) in the different water masses sampled along the
 1308 GA01 line. Median values for the water masses were as follows: LSW_{ib}= 0.37; LSW_{ir}=0.44; LSW_{WEB}=0.36;
 1309 ISOW_{east}=0.48; ISOW_{west}=0.58; DSOW_{lab}=0.42; DSOW_{ir}=0.47; NEADW=0.23; MW=0.22 mol mol^{-1} .



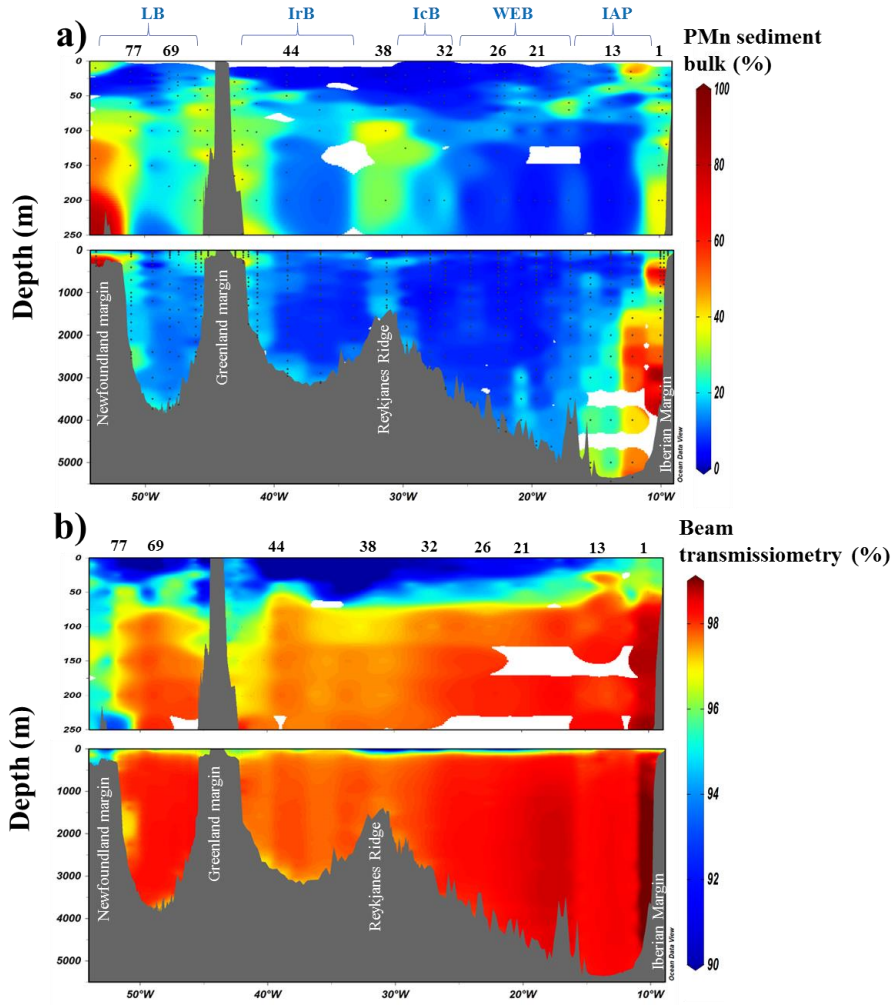
1310
 1311
 1312
 1313
 1314
 1315
 1316
 1317
 1318
 1319
 1320
 1321
 1322
 1323
 1324
 1325
 1326
 1327
 1328
 1329

1330 Figure 98: Scatter of the PFe/PAI ratio at the Iberian (red dots), East Greenland (black dots), West Greenland (green
1331 dots) and Newfoundland margins (blue dots). Dashed line indicate the UCC ratio (Taylor and McLennan, 1995).



1332
1333
1334
1335
1336
1337
1338
1339
1340
1341
1342

1343 Figure 109: Section of derived contribution of sedimentary inputs manganese bulk sediment proxy (a) and
 1344 transmissometry (b) along the GA01 section. Station IDs and biogeochemical region are indicated above the section
 1345 (a). This figure was generated by Ocean Data View (Schlitzer, R., Ocean Data View, odv.awi.de, 2017).



1346

1347

1348

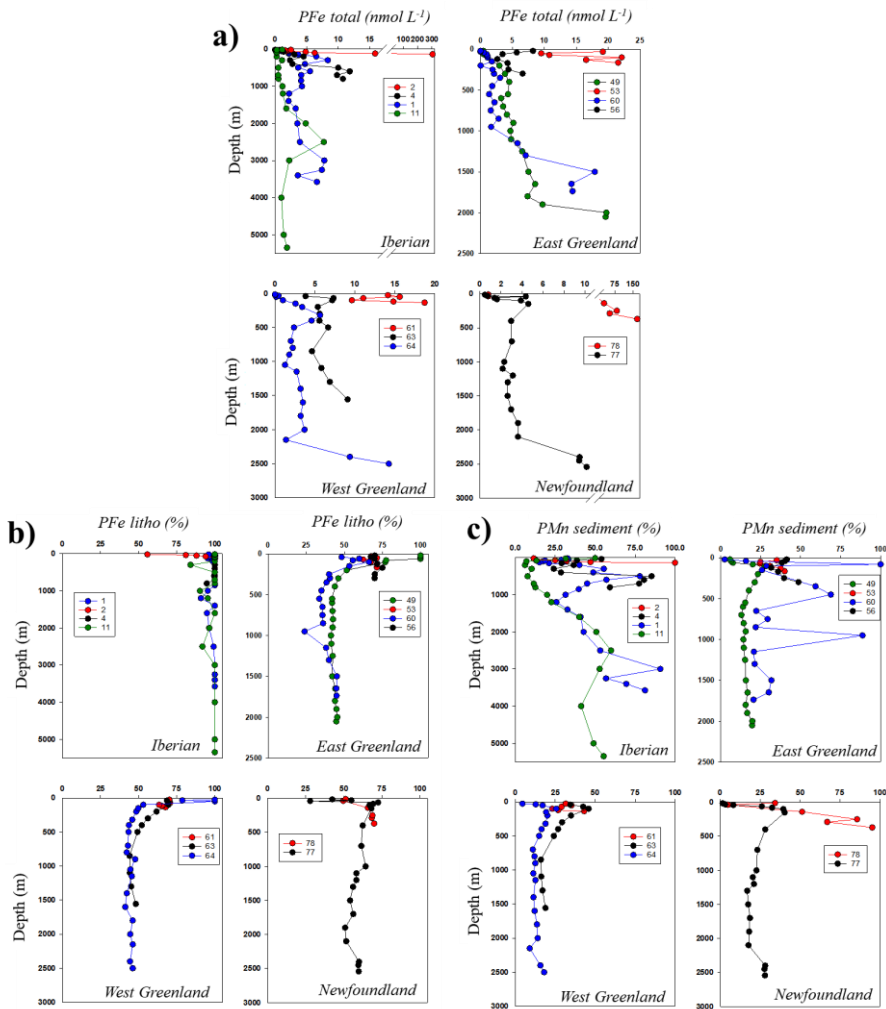
1349

1350

1351

1352
1353

Figure 140: Vertical profiles of PFe (nmol L⁻¹, a), lithogenic proportion of particulate iron (%), b) and sedimentary proportion of particulate manganese (%), c) at the Iberian, East-West Greenland and Newfoundland margins.



1354

1355

1356

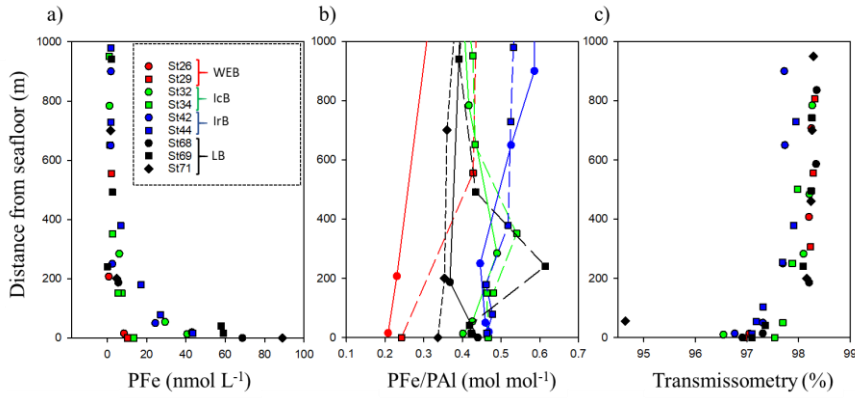
1357

1358

1359

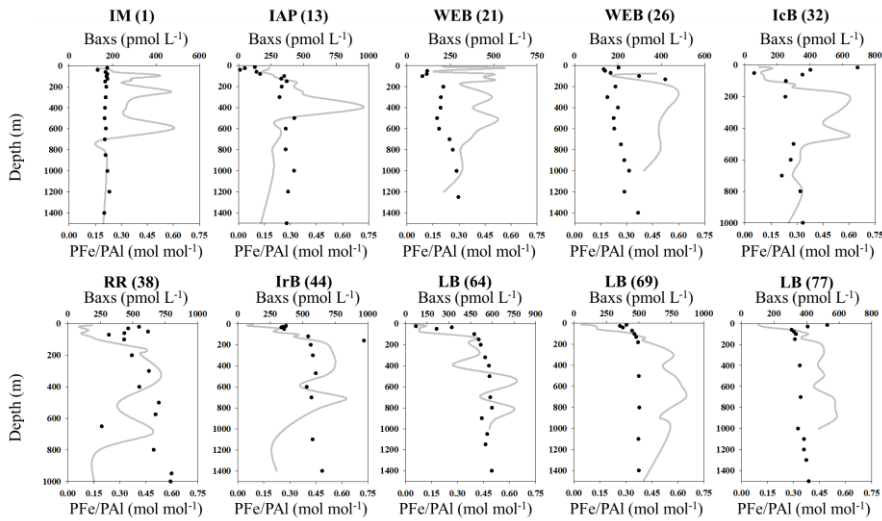
1360

1361 Figure 112: PFe total (a); PFe/PAI ratio (b) and beam transmissometry (%) as a function of depth above the seafloor
 1362 (m) at selected stations where a decrease in transmissometry was recorded.



1363
 1364
 1365
 1366
 1367
 1368
 1369
 1370
 1371
 1372
 1373
 1374
 1375
 1376

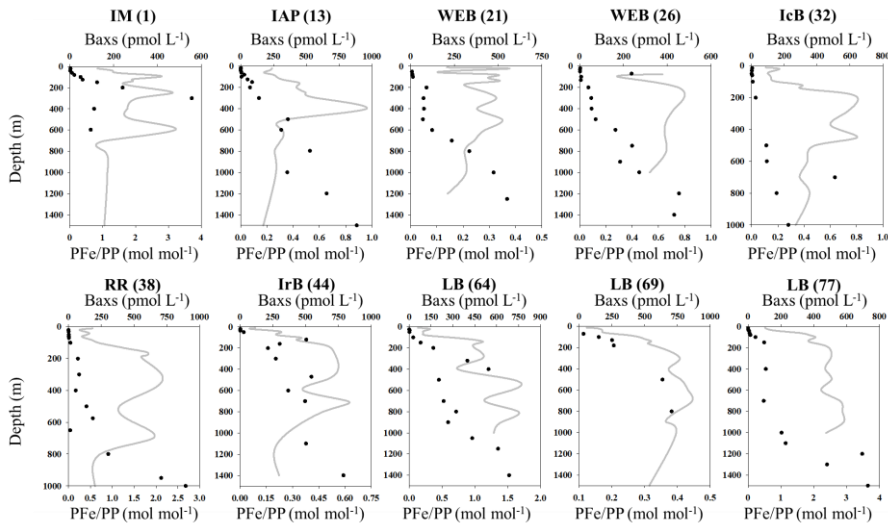
1377 Figure 13: Vertical profiles of B_{act} (grey line, data from Lemaitre et al., 2018a) superimposed with PFe/PAI molar
 1378 ratios (black dots) at stations sampled in the Iberian Margin (IM), Iberian Abyssal Plain (IAP), Western European
 1379 Basin (WEB), Iceland Basin (IcB), above the Reykjanes Ridge (RR), Irminger Basin (IrB), and Labrador Basin (LB).
 1380 Note that B_{act} concentrations over the background level of 180 pmol L⁻¹ are indicative of remineralisation processes
 1381 (Lemaitre et al., 2018a).



1382

1383

1384 **Figure 14: Vertical profiles of Baxs (grey line, data from Lemaitre et al., 2018a) superimposed with PFe_{bio}/PP molar**
 1385 **ratios (black dots) at stations sampled in the Iberian Margin (IM), Iberian Abyssal Plain (IAP), Western European**
 1386 **Basin (WEB), Iceland Basin (IcB), above the Reykjanes Ridge (RR), Irminger Basin (IrB), and Labrador Basin (LB).**
 1387 **Note that Baxs concentrations over the background level of 180 pmol L⁻¹ are indicative of remineralisation processes**
 1388 **(Lemaitre et al., 2018a).**



1389

1390

1391

		Fe	Al	P	Mn
Blank (nmol L ⁻¹)	5µm filter	0.072	0.100	0.511	0.003
	0.45µm filter	0.132	0.164	1.454	0.005
Limit of detection (nmol L ⁻¹)	5µm filter	0.011	0.030	0.365	0.001
	0.45µm filter	0.026	0.046	1.190	0.001
Recovery CRM (%)	BCR-414 (n=10)	88 ± 7			94 ± 7
	MESS-4 (n=5)	98 ± 14	97 ± 14	80 ± 30	110 ± 18
	PACS-3 (n=8)	101 ± 9	99 ± 14	91 ± 34	112 ± 11

Formatted: Centered

%-recovery	Al	P	Mn	Fe
BCR-414 (n=10)	-	-	94 ± 7	88 ± 7
MESS-4 (n=5)	97 ± 14	80 ± 30	110 ± 18	98 ± 14
PACS-3 (n=8)	99 ± 14	91 ± 34	112 ± 11	101 ± 9

Table 1: Blank and limit of detection (nmol L⁻¹) of the two filters and Certified reference material (CRM) recoveries during GEOVIDE suspended particle digestion.

Author	Year	Fraction	Location	Depth range	PFe	PAI	PMn	PP
This study		>0.45µm	N. Atlantic (>40°N)	All	bdl-304	bdl-1544	bdl-3.5	bdl-402
Barrett et al.	2012	0.4µm	N. Atlantic (25-60°N)	Upper 1000m	0.29-1.71	0.2-19.7		
Dammshausser et al.	2013	>0.2 µm	Eastern tropical N.A.	0-200		0.59-17.7		
Dammshausser et al.	2013	>0.2 µm	Meridional Atlantic	0-200		0.35-16.1		
Lam et al.	2012	1-51 µm	Eastern tropical N.A.	0-600	ND-12			
Lannuzel et al.	2011	>0.2 µm	East Antarctic	Surface		0.02-10.67	0.01-0.14	
Lannuzel et al.	2014	>0.2 µm	East Antarctic	Fast ice	43-10385	121-31372	1-307	
Lee et al.	2017	>0.8 µm	Eastern tropical S.Pacific	All	bdl-159	bdl-162	bdl-8.7	bdl-983
Marsay et al.	2017	>0.4 µm	Ross Sea	All	0.68-57.3	ND-185	ND-1.4	5.4-404
Milne et al.	2017	>0.45µm	Sub-tropical N.A.	All	ND-140	ND-800		
Ohnemus et al.	2015	0.8-51 µm	N. Atlantic	All	0-938	0-3600		
Planquette et al.	2009	>53 µm	Southern Ocean	30-340	0.15-13.2	0.11-25.5		
Schlosser et al.	2017	>1 µm	South Georgia Shelf	All	0.87-267	0.6-195	0.01-3.85	
Sherrill et al.	1998	1-53µm	Northeast Pacific	0-3557		0.0-54.2		
Weinstein et al.	2004	>53 µm	Labrador Sea	0-250	0.1-1.2	0.1-1.5		
Weinstein et al.	2004	0.4- 10µm	Labrador Sea	0-250	2.5	3.6	0.05	
Weinstein et al.	2004	>0.4 µm	Gulf of Maine	0-300	34.8	109		

Table 2: Concentration (in nmol L⁻¹) of trace elements (PFe, PAI, PMn and PP) in suspended particles collected in diverse regions of the world's ocean. Bdl: below detection limit, ND: non-determined.

1405

1406

1407